(4)

SECURITY CLASSIFICATION OF THIS PAGE (When Data Entered)

REPORT DOCUMENTATION PAGE		READ INSTRUCTIONS BEFORE COMPLETING FORM
1. REPORT NUMBER	2. GOVT ACCESSION NO.	3. RECIPIENT'S CATALOG NUMBER
4. TITLE (and Subtitle) A Probabilistic Model of Brittle Crack Formation		5. TYPE OF REPORT & PERIOD COVERED Interim April 1987-March 1988 6. PERFORMING ORG. REPORT NUMBER
7. AUTHOR(s) A. Moet, R. Dearth, H. Aglan, A. Chudnovsky and B. Kunin		8. CONTRACT OR GRANT NUMBER(s) N00014-86-K-0285
9. PERFORMING ORGANIZATION NAME AND ADDRESS Case Western Reserve University Cleveland, Ohio 44106-2699		10. PROGRAM ELEMENT, PROJECT, TASK AREA & WORK UNIT NUMBERS
11. CONTROLLING OFFICE NAME AND ADDRESS		12. REPORT DATE July 1988 13. NUMBER OF PAGES 63
14. MONITORING AGENCY NAME & ADDRESS(if different from Controlling Office) Office of Naval Research Arlington, Virginia 22217		15. SECURITY CLASS. (of this report) Unclassified 15a. DECLASSIFICATION/DOWNGRADING SCHEDULE

16. DISTRIBUTION STATEMENT (of this Report)

Approved for public release; distribution unlimited

17. DISTRIBUTION STATEMENT (of the abstract entered in Block 20, if different from Report)

18. SUPPLEMENTARY NOTES

19. KEY WORDS (Continue on reverse side if necessary and identify by block number)

C/C composite; probabilistic fracture; strength field

20. ABSTRACT (Continue on reverse side if necessary and identify by block number)

PLEASE SEE REVERSE

DD FORM 1 JAN 73 1473 EDITION OF 1 NOV 65 IS OBSOLETE
S/N 0102-LF-014-6601

SECURITY CLASSIFICATION OF THIS PAGE (When Data Entered)

20. ABSTRACT

Multiple experiments on macroscopically identical 3D carbon-carbon (C/C) composite specimens show that the fracture behavior displays the main features of a stochastic process which reflects the random nature of the strength field. The critical load is random and a sample set of crack trajectories displays a Poisson's type diffuse character. Crack trajectories are unique for each individual experiment (no two coincide). The crack appears to propagate stepwise (a sequence of local failures) through a random field of defects which is constrained by the orthotropic architecture of the yarn bundles. As such, the strength field cannot be approximated by a single parameter, a specific fracture energy $2\gamma=J_{1C}$.

In our previous report, we presented the mathematical foundation of a probilistic model of brittle crack formation. The model combines the concepts and formalism of conventional fracture mechanics with the concepts and formalism of stochastic processes. The strength field, i.e., the specific fracture energy $2\gamma=J_{1C}$ in fracture mechanics, is now considered as a fluctuating field which is described by a pointwise Wiebull distribution $F(\gamma)$, the correlation distance r_o and the crack diffusion coefficient. Several refinements of the model are introduced. The probability that a crack propagates along a specific path, "chosen" from all possible paths, from an initial point to a final point is introduced through the "crack propagator" concept. Of course, the crack diffusion coefficient uniquely determines the set of all possible crack paths. Equations are derived to predict the probability of crack penetration depth in terms of the energy release rate (stress-strain distribution), the crack diffusion coefficient and the correlation distance (statistical features of the strength field) for stable (crack arrest) and unstable (critical crack) configurations.

Guided by these theoretical developments, an experimental methodology is designed to evaluate the parameters called upon by the theory and to examine its predictive power. A model material whose fracture behavior is well understood (PMMA) was used. The experiment employs crack arrest (stable) configuration. From the statistical characteristics of the load (or displacement) and crack arrest length, and the correlation distance (defined from fractographic examination), the strength field parameters γ_{ave} and α are deduced from the proposed model.

carbon [illegible] (27)

A PROBABILISTIC MODEL OF BRITTLE CRACK FORMATION

A. Moet, R. Dearth and H. Aglan
Department of Macromolecular Science
Case Western Reserve University
Cleveland, Ohio 44106

A. Chudnovsky and B. Kunin
Department of Civil Engineering, Mechanics
and Metallurgy
University of Illinois at Chicago
Chicago, Illinois 60680

Technical Report

Prepared for

Office of Naval Research
Arlington, Virginia 22217

Monitor, Dr. L.H. Peeble, Jr.
Contract No. N00014-86-K-0285

July, 1988

Table of Contents

CHAPTER I

CRACK PROPAGATION IN CARBON-CARBON COMPOSITES

H. Aglan and A. Moet
Department of Macromolecular Science
Case Western Reserve University
Cleveland, Ohio 44106

1. Introduction

Fracture mechanics delivers the methodology to compensate the inadequacies of conventional design concepts based on tensile strength, yield strength or buckling stress particularly when there is the likelihood of cracks. At present, fracture mechanics concepts are well developed and standard procedures are established to determine fracture toughness parameters on the basis of linear elastic or nonlinear theories. Both theories deal with homogeneous, isotropic materials whose strength field may be well approximated by a single (fracture toughness) parameter , be it the critical stress intensity factor K_{Ic} or the critical energy release rate J_{1c}. Carbon-carbon composites do not fit this description. The course orthotropic texture of the relatively large yarn bundles coupled with the extreme anisotropy of the graphitic matrix play a major role in determining the microstructural character and behavior of the composite. An important consequence of such anisotropy is the microcracking network induced by thermal stresses during manufacturing [1, 2]. These microstructural complexities violate the fundamental assumptions of a continuum upon which fracture mechanics is founded. The few reported studies which attempted to characterize the fracture resistance of carbon-carbon composites [3-9] attest to the inappropriateness of the conventional fracture mechanics methods. In this regard, the need concluded by Jortner, in a recent symposium on Thermomechanical Behavior of High Temperature Composite [10], for innovative mathematical modeling ought to be addressed.

The very nature of carbon-carbon composite indicates that the strength field is heterogeneous and can not be characterized by a single parameter. Recognizing this basic fact, we introduced the basic mathematical structure of a probabilistic model for brittle crack propagation in our previous report. The physical assumption underlying our approach is that brittle fracture of solids is controlled by a random field of microdefects. The strength of such a field, i.e., the specific fracture energy 2γ in conventional fracture mechanics, is now considered as a random field. The crack advances through the weakest "links" in the random field. It results in a randomly tortuous crack trajectory. The crack diffusion coefficient is introduced as an integral characteristic of such tortuosity [11-13].

Since the crack propagates through the weakest "links", the values of γ-field along an actual crack trajectory represent minima in the specific fracture energy. This, in accordance with the statistics of extremes, suggest a Wiebull distribution for γ at every point of the crack trajectory. The distribution is characterized by three parameters: γ_{min}, γ_{ave} and α, the shape parameter. The values of γ at two different points are generally described by a joint distribution function. However, when the two points are separated by a distance $r > r_o$, the values of γ at the two points are mutually independent. The distance r_o is the correlation distance.

Chudnovsky and Kunin derived the probability of crack penetration depth under a specified displacement in terms of the strength field parameters and the energy release rate [11]. An experiment was designed to examine the validity of the proposed theory. Results of

these experiments are discussed in Chapter III. In this Chapter, the phenomenological features of crack propagation in 3D C/C composites are described. These results are sought to assess the applicability of the proposed theoretical model and to guide further refinement of the theory.

2. Materials and Testing

Two carbon-carbon composites were considered in this work. Both materials are three dimensions C/C composites. They are G20-6G after graph. 7 and G20-4G after graph. 5, obtained from the Aerospace Corporation. The average thickness for each billet is about $\frac{1}{4}$". The G20-6G is a higher density composite while the G20-4G is a lower density.

Different specimen geometries such as compact tension and tapered double cantilever beam were attempted to carry out fracture tests on the 3-D carbon composites. In spite of reinforcing the holes of the specimen, failure occurred at the grips. A three-point bend specimen under monotonic loading was then chosen to conduct the fracture testing. The test specimens were machined into 56 X 14 mm beams from the billet sections as illustrated in Fig. 1. A 0.38 mm thick milling cutter was used to introduce a 3mm notch at the middle of each specimen.

Fracture testing was carried out at room temperature using an MTS testing system equiped with a 1 kip load cell. The test was run using displacement control with a cross-head speed of 50μ/min. A specially designed Instron stiff steel load fixture was used to insure minimum machine compliance.

The load versus the load-point displacement (LPD) curves were generated by continuously monitoring the load and crosshead displacement

during tests. A clip gauge was also used to monitor the load versus the crack opening displacement (COD). Both load vs. LPD and load vs. COD curves were plotted instantaneously during the tests on X-Y plotters. The data were also digitized and stored using a digital computer system attached to the testing machine.

The tip of the notch was viewed using a travelling optical microscope. A video system was attached to the microscope in order to obtain interval records of crack propagation and to record any damage events which could be observed.

Nine macroscopically identical specimens of the composite B7 as well as five specimens of composite B5 were fractured under identical test conditions.

One test on composite B5 was stopped after a first major drop in the load was observed. The sample was then examined using SEM to identify the damage events associated with that drop in the load.

3. Results

A typical load vs. LPD curve for both composites is shown schematically in Fig. 2. Actual load vs. LPD and load vs. COD curves for one sample of the B7 composite are shown in Figures 3 and 4, respectively. Both curves exhibit the same trend. At the beginning there is a linear portion followed by another of increased nonlinearity. After a peak is reached at P_2 and Δ_2, major damage events appear to have occurred causing successive load drops (Figures 3 and 4). Each load drop is preceded by an approximately constant load plateau.

A histogram of maximum loads P_2 and the corresponding displacement Δ_2 of the nine identical specimens of the B7 composite is shown in Fig. 5. The wide scatter, again, attests to the random nature of the strength field.

SEM observations reveal the tortuous nature of the fracture path and how is it dictated by the material's architecture. Figure 6 displays a composite micrograph showing the entire fracture path of one of the B7 composite specimens. The crack appears to have advanced by a series of discrete steps involving interlaminar and cross laminar fracture processes. In other words, the crack diffusion into the random field is constrained by the yarn bundles. Interlaminar fracture proceeds until "a weak link" in the yarn permits a cross laminar advance.

Although a final drop of the load-displacement curve indicated ultimate failure, the two halves of the specimen remained together (Fig. 6). This indicates that the fracture "surface" is not traction free; a feature that deviates from the basic concepts of fracture mechanics. Mechanical interlocking and yarn pull-out resistance appear to play a role in the fracture processes.

To ascertain the crack path in Fig. 6, the same specimen was separated manually and one half was re-examined in the scanning electron microscope. A micrograph of this half is shown in Fig. 7. The discrete "steps" of crack advance can now be traced. The crack difussion is constrained by the yarn bundles.

Crack trajectories at the specimen surface (side view) were observed from shadow graphs obtained with angular illumination ($\sim 30°$). This

procedure was followed to observe only surface projection of the crack path. An assembly of the nine trajectories is shown in Fig. 8. These trajectories possess two specific discriminating features when compared with those obtained form short fiber composite [13] or PMMA [14]. Firstly, the diffusive crack behavior appears to be constrained (non-Brownian) and secondly, deviation of the trajectories from the X-axis increases up to a certain crack depth then decreases towards the loading point. The results of Fig. 6-8 suggest further refinement of the proposed model as will be discussed subsequently.

Specimens prepared from the B-5 composite (lower density) display similar behavior. Typical load-displacement curves for B-7 and B-5 are plotted in Fig. 9. As expected, the B-5 specimen shows similar LPD but at lower loads. Again, this result indicates that the role of the composite "main frame" architecture dictates the general fracture behavior.

In an attempt to explore the fracture events associated with load-drops, a B-5 specimen was monotonically loaded until the first load drop occurred then was unloaded. The load vs. LPD is shown in Fig. 10 and the load vs. COD is shown in Fig. 11. The specimen was then examined in scanning microscope. A SEM micrograph is shown in Fig. 12. Significant crack propagation is observed. The crack initiated from the center of the notch across a circumferential yarn bundle, inter-facially along the first interface encountered to a certain length, at which it propagates tortuously across yarn to be arrested there. This exploratory experiment suggests the availability of information

necessary to define "elementary" fracture processes responsible for the unusual load-displacement behavior.

4. Discussion

The results outlined in the previous section serve two purposes: (1) to probe the specific nature of fracture processes in C/C composite, and (2) to explore the type of information available from fracture experiments.

Indeed, the strength field of C/C composite can not be approximated by a single (fracture energy) parameter and ought to be treated as a random field. Hence, a probabilistic approach ought to be developed. For this purpose, a model for brittle crack formation evolved [11]. Further refinement of the model is presented in Chapter II of this report. Experimental procedures and analytical methods were developed to employ the theory. In Chapter III, the methodology of evaluating the random field parameters from crack arrest experiments is described.

As evident from the present study, C/C composites display the main ingredients of probabilistic (stochastic) fracture. However, the results reveal that the material architecture imposes certain specificities which include:

(1) The load-displacement curves of C/C composite display characteristically discrete steps which appear to reflect failure of individual yarn bundle or a group of yarns. Failure of an individual yarn is considered to be an elementary event of the fracture process. The specific energy of such events constitutes the γ-field. A link between

the statistics of the load-displacement steps and that of individual yarn fracture ought to be established.

(2) The sample set of crack trajectories (Fig. 8) displays Poisson's type features. In our current model Wiener's type formalism is employed to characterize the set of all possible crack trajectories Ω. This requires reformulating the probabilistic measure μ on Ω and establishing integration procedure over Ω.

(3) The crack path (Fig. 12) clearly shows that evaluation of the stress-strain singularity at the crack tip, a necessary excercise to evaluate the energy release rate along a given path, requires the search for an innovative technique for stress analysis. Perhaps, a brittle lacquer or a photoelastic technique may produce useful information to perform the required stress analysis.

5. Conclusions

(1) Fracture of C/C composite displays the main features of probabilistic brittle fracture which can be described by the probabilistic model of brittle crack formation.

(2) The crack trajectories reflect the constrains imposed by the 3D yarn bundles. This would require the application of Poisson's formalism to characterize the set of possible crack trajectories.

(3) The load-displacement curve displays characteristically discrete steps which are believed associated with elementary fracture events.

REFERENCES

1. J. Jortner, Carbon, 24, 603, 1986.

2. L. Peebles, R. Meyer and J. Jortner, Proceedings of the 2nd International Conference on Composite Interface, Cleveland, Ohio, June, 1988.

3. M. Jenkins, J. Mikami, T. Chang and A. Okura, SAMPE Journl, May 1988 page 32.

4. M. Jenkins, A. Kobayashi, A. White and R. Bradt, Int. J. Fracture, 34, 281, 1987.

5. D. Phillips, J. Composite Materials, 8, 130, 1974.

6. T. Guess and W. Hoover, J. Composite Materials, 7, 2, 1973.

7. L. Hettche and T. Tucker, Crack and Fracture, ASTM STP, 601, 109, 1976.

8. D. Adams and E. Odom, Composites, 18, 5, 1987.

9. Y. Kagawa, S. Utsunomiya and M. Imaizumi, Proceeding of the 30th Japan Congress on Material Research, 1987.

10. J. Jortner, Ed., "Thermomechanical Behavior of High-Temperature Composites", ASME, New York, November, 1982.

11. Chudnovsky and Kunin, J. Appl. Phys., 62, 10, 1987.

12. Chudnovsky and Kunin, "A Probabilistic Model of Brittle Crack Formation", to be published.

13. M. Mull, A. Chudnovsky and A. Moet, Philosophical Magazine A, 56, 419, 1987.

14. R. Dearth, H. Aglan, A. Moet, B. Kunin and A. Chudnovsky, Chapter III of this report.

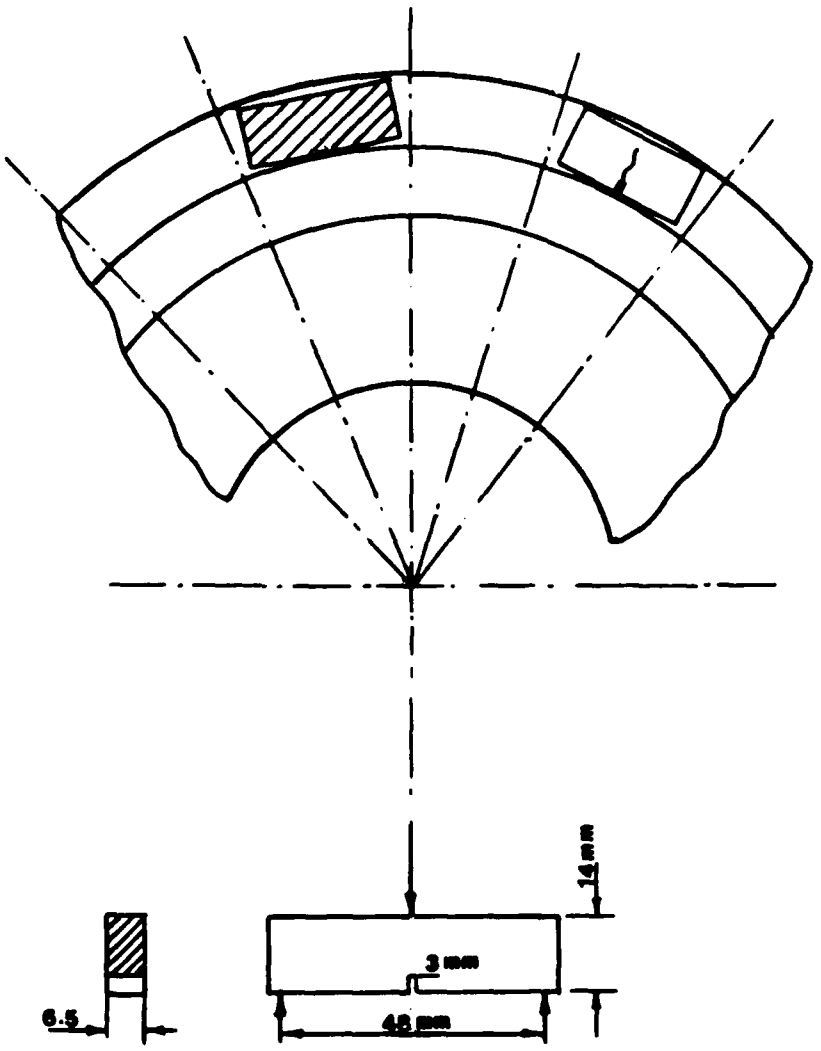

Fig. 1 Specimen geometry and orientation

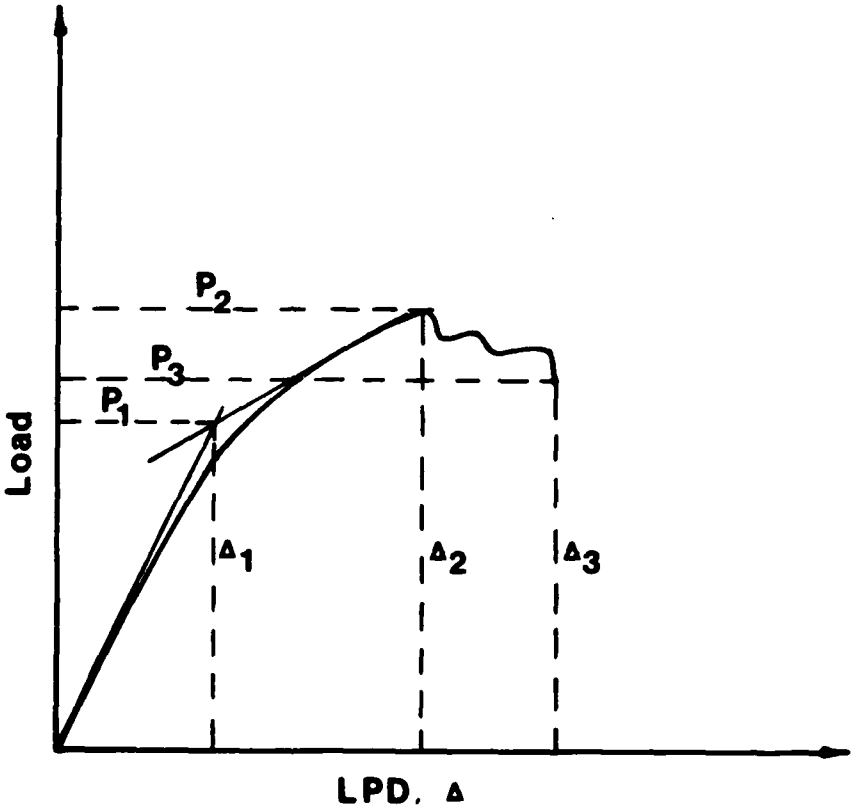

Fig. 2 Typical load-deflection curve for 3-point bending of C/C composites

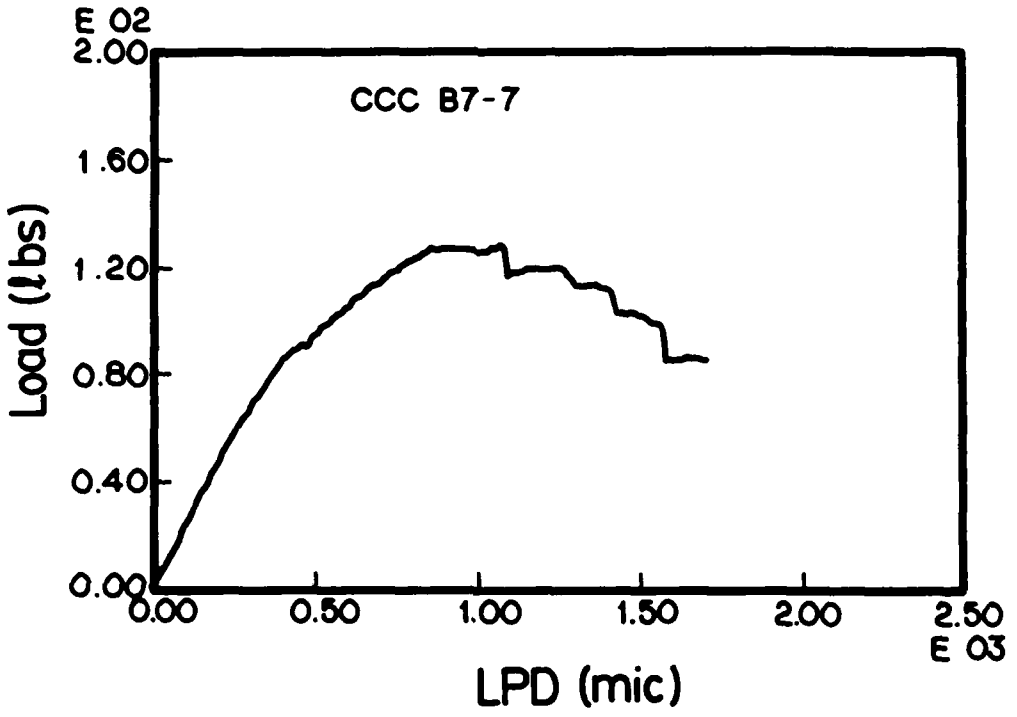

Fig. 3 Load versus load point displacement (LPD) for one specimen of the B-7 C/C composite

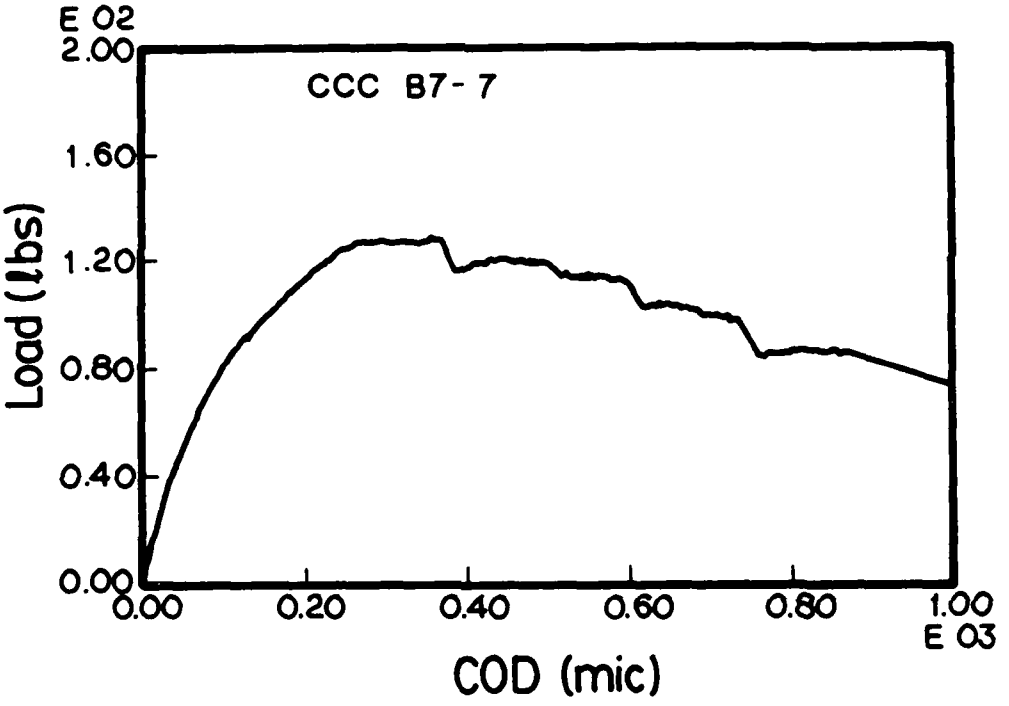

Fig. 4 Load versus crack opening displacement (COD) for one specimen of the B-7 C/C composite

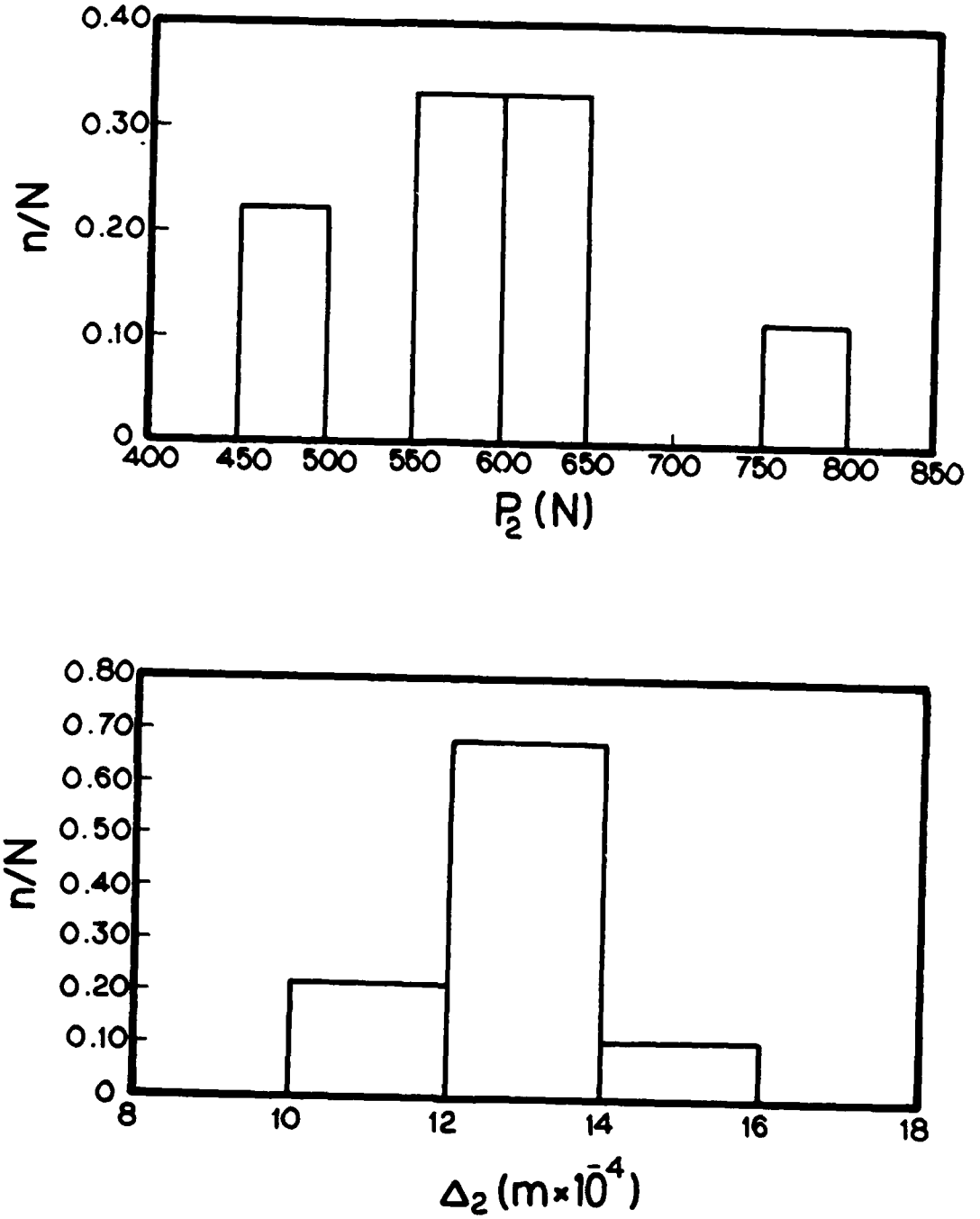

Fig. 5 Histogram of the max load, P_2, and its corresponding LPD for the B-7 C/C composite

Fig. 6 A crack trajectory of one specimen of the B-7 C/C composite

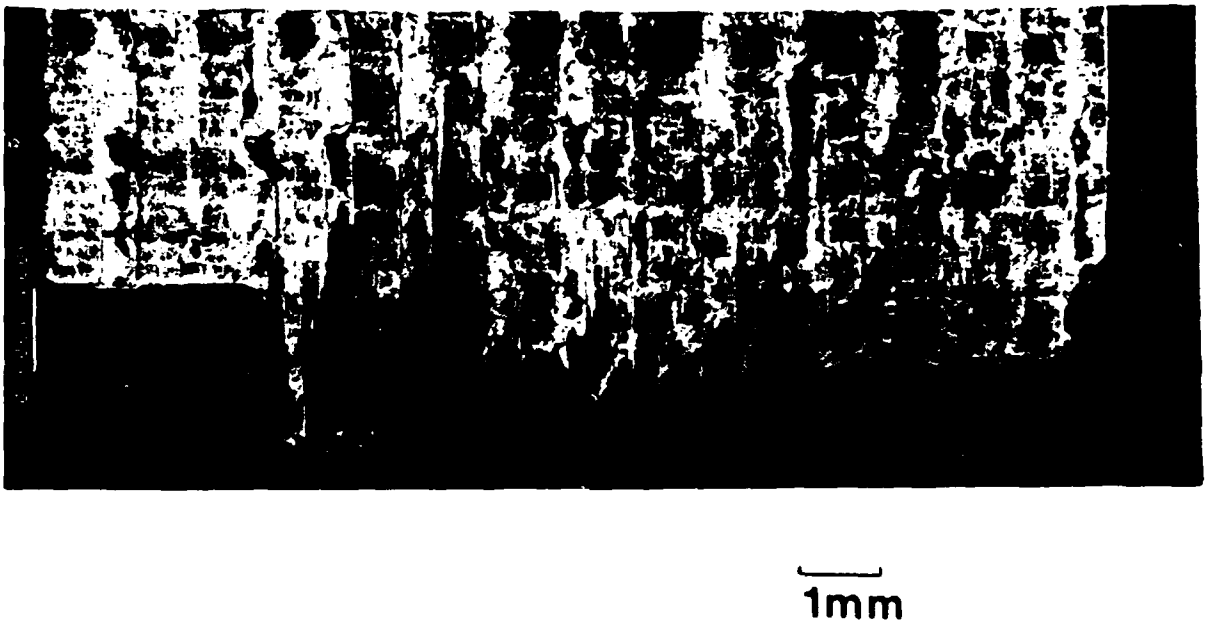

Fig. 7 The upper half of the specimen in Fig. 6 after separation

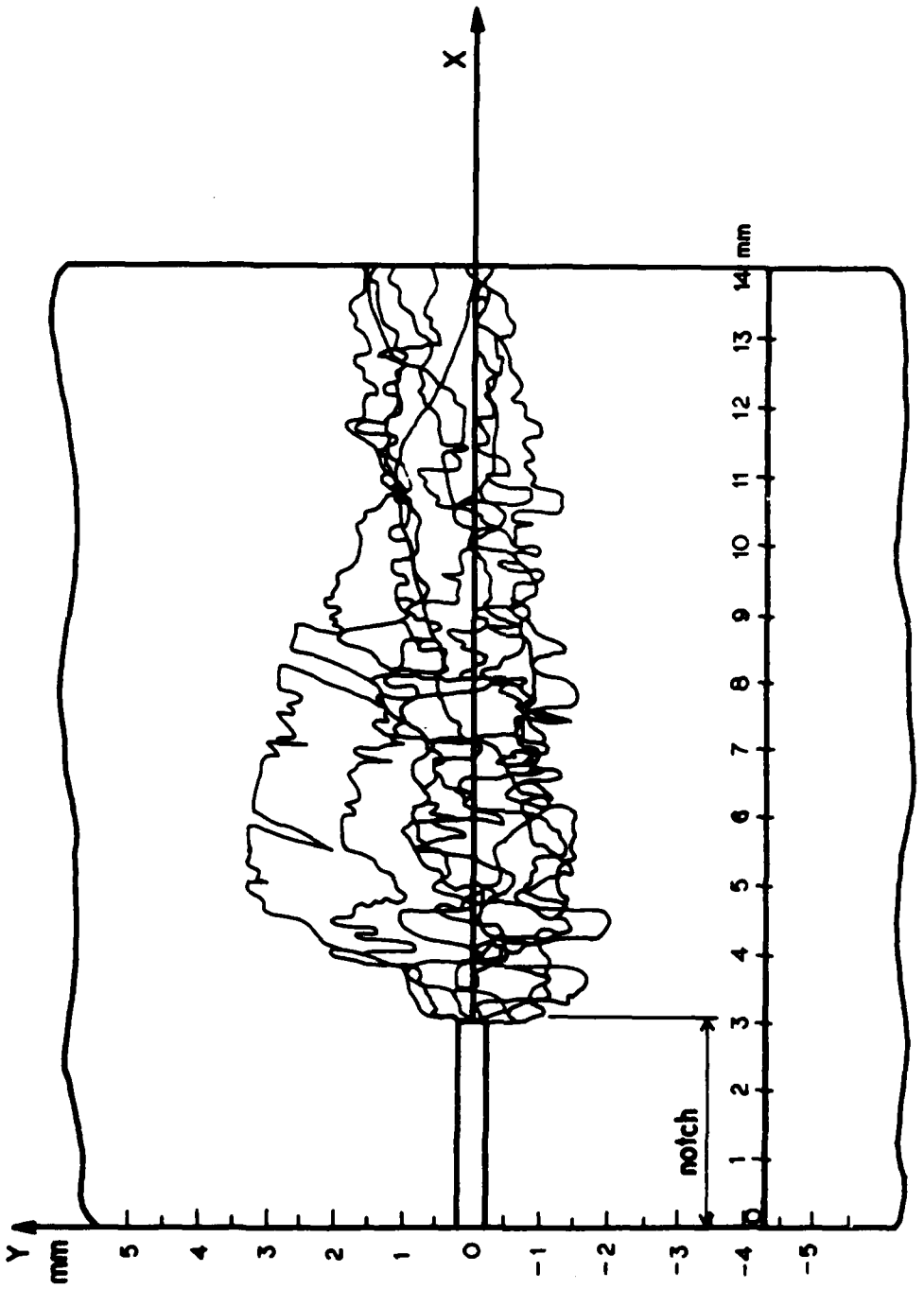

Fig. 8 Crack trajectories of nine identical 3-point bend specimens superimposed onto the same set of coordinate axes

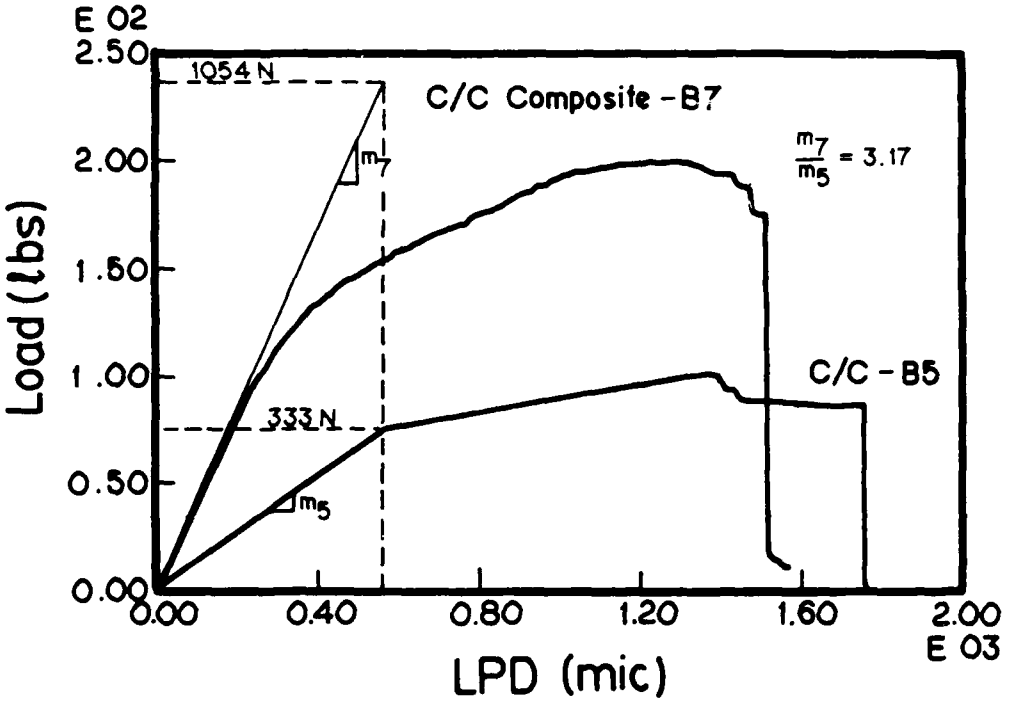

Fig. 9 Load versus LPD for two identical samples of B-7 and B-5 C/C composites

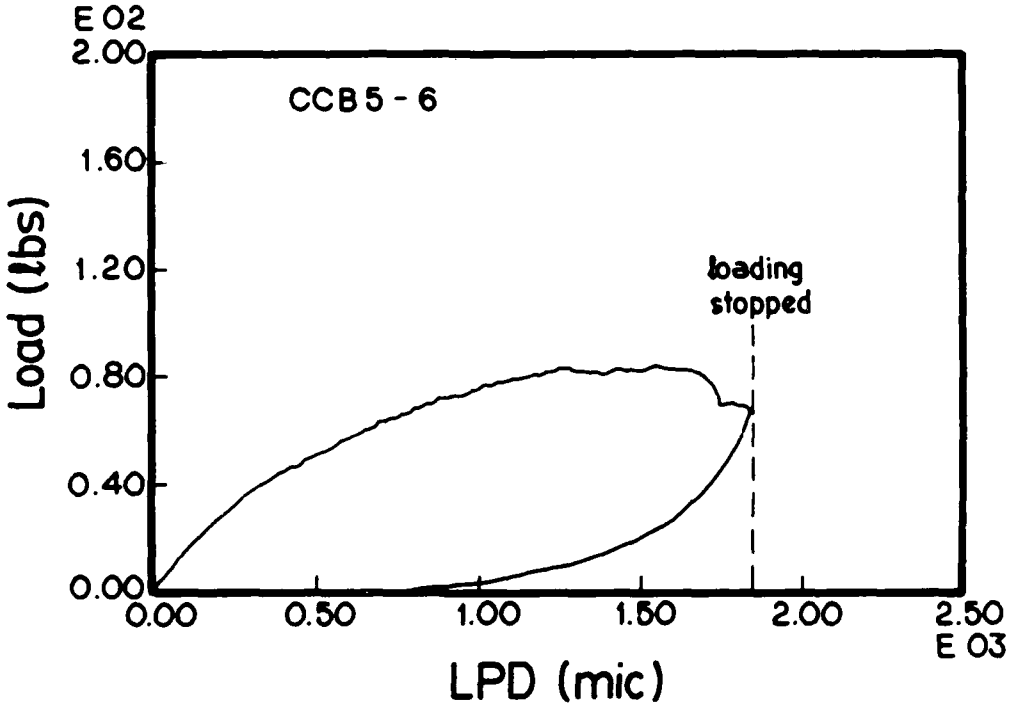

Fig. 10 Load versus LPD for one specimen pf B-5 C/C composite. The specimen was unloaded after a major drop in the load.

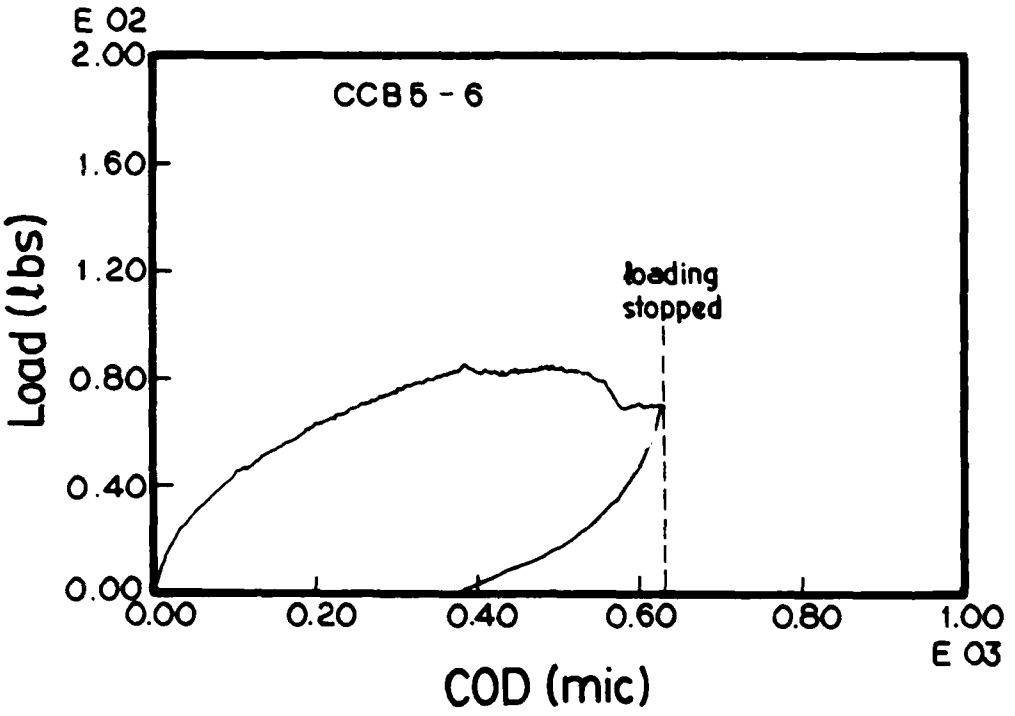

Fig. 11 Load versus COD for one specimen pf B-5 C/C composite. The specimen was unloaded after a major drop in the load.

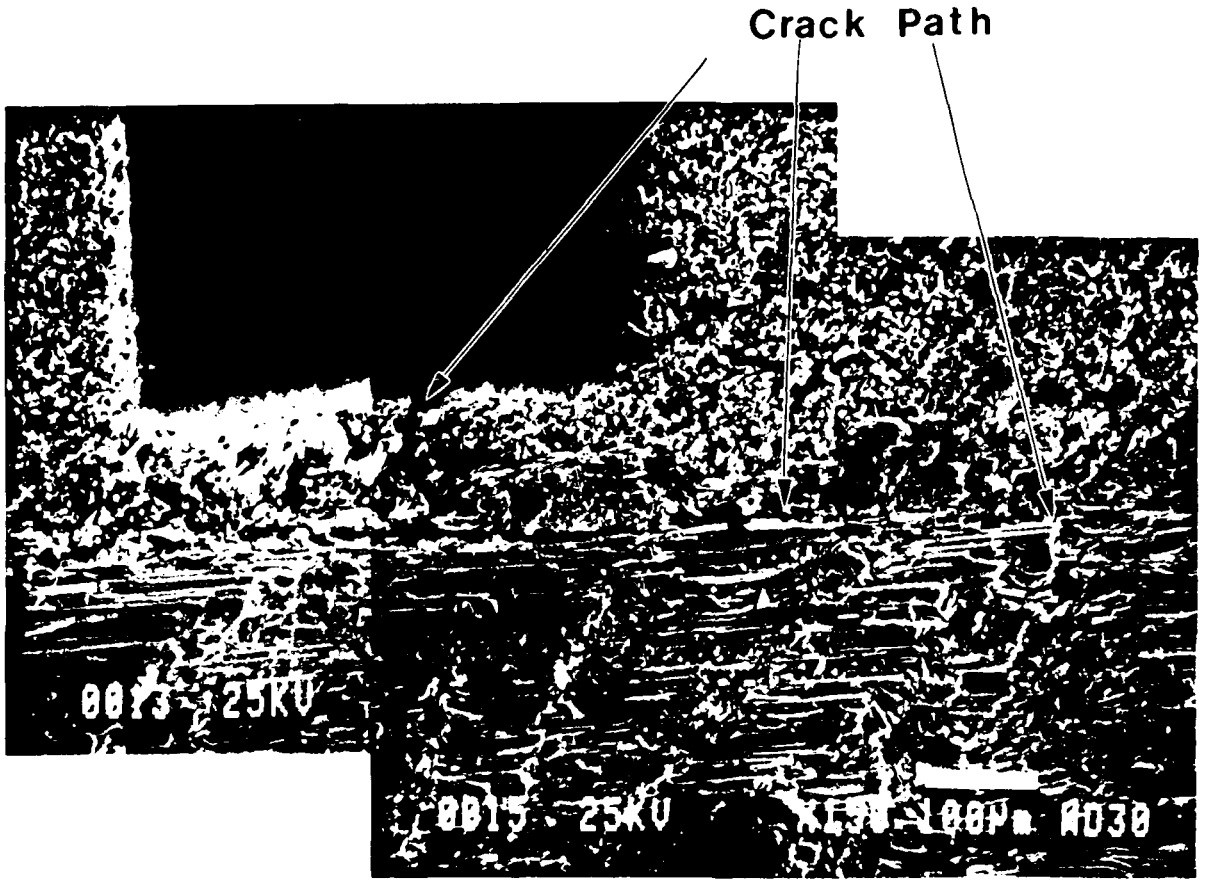

Fig. 12 A micrograph of a B-5 C/C composite specimen illustrating the crack jump which is associated with the first major drop in the load

CHAPTER II

A PROBABILISTIC MODEL OF BRITTLE CRACK FORMATION, II

A. Chudnovsky and B. Kunin
Department of
Civil Engineering, Mechanics, and Metallurgy
University of Illinois at Chicago
Chicago, Illinois 60680

A PROBABILISTIC MODEL OF BRITTLE CRACK FORMATION, II

A. Chudnovsky and B. Kunin
Department of Civil Engineering,
Mechanics, and Metallurgy
University of Illinois at Chicago
Chicago, Illinois 60680

1. INTRODUCTION

The physical assumption underlying our approach is that the brittle fracture of solids is controlled by a random field of microdefects. We are interested in a characterization of this field only as far, as it relates to fracture phenomena. We take a random field of specific fracture energy γ as a representative characteristic of the defect population.

We address the following question: how the scatter of such macroscopical parameters, as critical load, critical crack length, crack trajectories, etc. are related to the statistics of the γ-field. Our objective is a reconstruction of the statistical parameters of the γ-field on the basis of observed quantities.

2. CRACK PROPAGATOR

Let us consider a crack ω_o in a two-dimensional solid. Suppose that the crack tip is at a point $\vec{x}$ (see Fig. 1). We define crack propagator $P_{\omega_o}(\vec{x},\vec{X})$ as the probability that the crack ω_o extends from $\vec{x}$ through another point $\vec{X}$.

Multiple experiment on crack extension under *macroscopically* identical conditions demonstrates that crack trajectories are unique for each individual experiment (no two coincide). More importantly, in a given test, any of the trajectories observed in other (macroscopically) identical tests should be

viewed as a priori possible. Statistical analysis of the observed crack trajectories allows one to formulate assumptions about the set Ω of all possible crack trajectories (connecting $\vec{x}$ and $\vec{X}$).

We now assume that only one crack is formed in each specimen (single path fracture).[α] Then the crack propagator $P_{\omega_o}(\vec{x}, \vec{X})$ can be written as

$$P_{\omega_o}(\vec{x},\vec{X}) = \sum_{\Omega} P_{\omega_o}(\vec{x},\vec{X}|\omega)\, P_{\omega_o}\{\omega\} \tag{1}$$

where $P_{\omega_o}\{\omega\}$ is the probability that the crack 'chooses' a path ω among all possible paths extending ω_o from $\vec{x}$ to $\vec{X}$, and $P_{\omega_o}(\vec{x},\vec{X}|\omega)$ is the conditional propagator, i.e., the conditional probability that the crack reaches $\vec{X}$ if it grows along a particular ω.

In a continuum based model, the space Ω is uncountable, and so the sum in Eq. (1) is substituted by an integral:

$$P_{\omega_o}(\vec{x},\vec{X}) = \int_{\Omega} P_{\omega_o}(\vec{x},\vec{X}|\omega)\, d\mu(\omega) \tag{2}$$

Thus determination of the crack propagator is reduced to the following tasks: selection of an adequate crack trajectory space Ω and the probability measure $d\mu(\omega)$ on Ω as well, as evaluation of the conditional crack propagator $P_{\omega_o}(\vec{x},\vec{X}|\omega)$.

It is observed for typical test conditions, that a preferred direction exists with respect to which the crack trajectories are graphs, $\xi_2 = \xi_2(\xi_1)$ (see Fig. 1, which represents schematically a trial set of possible crack extensions from $\vec{x}$ to $\vec{X}$).

In this paper, as in Ref. 1, we restrict ourselves to a 'diffusion' approximation, i.e., we model crack trajectories by graphs of one-dimensional Brownian motion $\omega = \omega(\xi_1)$, $x_1 \le \xi \le X_1$, $\omega(x_1) = x_2$, $\omega(X_1) = X_2$ ($\Omega_{\vec{x},\vec{X}} = \{\omega\}$ will denote the space) and choose $d\mu(\omega)$ to be a conditional Wiener measure[β]

$d^{(D)}_{\vec{x},\vec{X}}(\omega)$ referring to the parameter $D > 0$, as a 'crack diffusion coefficient' (cf. Eqs. (10a,13a)); D reflects the tendency of crack trajectories to deviate from the ξ_1-axis and is experimentally measurable[7]. In the diffusion approximation, evaluation of D uniquely determines the set of all possible crack trajectories as well, as the measure $d\mu(\omega)$.

Determination of the conditional crack propagator $P_{\omega_o}(\vec{x},\vec{X}|\omega)$ depends on the mechanism of crack growth. One can visualize various sequences of local failures leading to the crack extension along ω from $\vec{x}$ to $\vec{X}$. Following Ref. 1, we consider crack formation (along ω) as a sequence of local failures immediately ahead of a current crack tip. This contrasts possibilities of crack growth by merging with local failures that occurred away from the crack tip.

Being concerned with brittle fracture, we adopt a Griffith type criterion of infiniteimal crack advance along a trajectory ω: at a current crack tip position $\vec{\xi}$, the potential energy release rate $J_\omega(\vec{\xi})$ should exceed the specific fracture energy $2\gamma(\vec{\xi})$.

The evaluation of $P_{\omega_o}(\vec{x},\vec{X}|\omega)$ based on the above criterion is the same as that presented in Ref. 1. It is assumed that γ is a statistically homogeneous random field whose values are independent at distances exceeding certain r, which is much smaller than the crack size. Then the probability that the criterion of infinitesimal crack advance ($J_\omega > 2\gamma$) is met at every point of ω is given by (see Ref. 1, Appendix)

$$P_{\omega_o}(\vec{x},\vec{X}|\omega) = \exp\left\{ - \int_{x_1}^{X_1} P_{\omega_o}\{2\gamma \geq J_\omega(\xi_1)\} \frac{d\xi_1}{r} \right\} \tag{3}$$

Finally, it is assumed[1] that values of γ along possible crack trajectories represent minimal values of the γ-field and therefore should obey one of the distributions of extremies. The Weibul distribution is a natural choice, since γ is a non-negative quantity[δ]. Thus the distribution function for γ is

$$F(\gamma) = \begin{cases} 1 - \exp\left[-\left(\dfrac{\gamma-\gamma_{min}}{\gamma_o}\right)^{\alpha}\right] & , \quad \gamma \geq \gamma_{min} \\ 0 & , \quad \gamma < \gamma_{min} \end{cases} \tag{4}$$

where $\gamma_{min} \geq 0$, $\gamma_o > 0$ and $\alpha > 0$ are empirical constants.

Combining Eqs. (2-4), one obtains the following expression for the crack propagator[ε]

$$P(x,X) = \int\limits_{\Omega_{\vec{x},\vec{X}}} \exp\left\{ -\int_{x_1}^{X_1} \exp\left[-\left(\frac{J_\omega(\xi_1)/2-\gamma_{min}}{\gamma_o}\right)^{\alpha}\right]\frac{d\xi_1}{r} \right\} \tag{5}$$

$$\times d\mu^{(D)}_{\vec{x},\vec{X}}(\omega) \quad .$$

3. CRACK DIFFUSION EQUATIONS

The energy release rate $J_\omega(\xi_1)$ is a functional of the crack trajectory ω. It can be approximated by a function $J(\xi_1,\omega(\xi_1))$ of the crack tip coordinates (see Ref. 1, p. 4126). Such an approximation allows one to represent the functional integral in Eq. (5) as the solution of a partial differential equation. Moreover, it is known that $P(\vec{x},\vec{X})$ given by Eq. (5) [with $J_\omega(\xi_1)$ substituted by $J(\xi_1,\omega(\xi_1))$] is the solution of each of the following two boundary value problems:

$$\partial_{X_1} P(\vec{x},\vec{X}) = \frac{D}{2} \partial^2_{X_2} P(\vec{x},\vec{X}) - \frac{1}{r} U(\vec{X}) P(\vec{x},\vec{X}) \tag{6a}$$

$$P(\vec{x},\vec{X})\Big|_{X_1 = x_1} = \delta(x_2 - X_2) \tag{6b}$$

$$P(\vec{x},\vec{X}) \to 0 \ , \quad \text{as} \quad X_2 \to \pm\infty \ , \quad X_1 > x_1 \tag{6c}$$

and

$$\partial_{x_1} P(\vec{x},\vec{X}) = \frac{D}{2}\ \partial^2_{X_2}\ P(x,X) + \frac{1}{r}\ U(x)\ P(x,X) \tag{7a}$$

$$P(\vec{x},\vec{X})\Big|_{x_1 = X_1} = \delta(x_2 - X_2) \tag{7b}$$

$$\partial_{x_2} P(\vec{x},\vec{X}) \to 0 \ , \quad \text{as} \quad x_2 \to \pm\infty \ , \quad x_1 < X_1 \ , \tag{7c}$$

where the 'potential' $U(\vec{\xi})/r$ expresses the probability density (in ξ_1) of the crack arrest ($J(\xi) \leq 2\gamma$) at a point $\vec{\xi}$; $U(\vec{\xi})$ is directly related to the Weibull distribution for γ and is given by (see Eq. 4)[θ] and Footnote[ε])

$$U(\xi) = \exp\left[-\left(\frac{J(\xi)/2 - \gamma_{min}}{\gamma_o}\right)^{\alpha}\right] \ . \tag{8}$$

Apparently, U accounts for the stress-strain distribution (through the energy release rate J), while the crack diffusion coefficient D and the correlation distance r reflect only the statistical features of the fracture processes.

We apply the above equations to two essentially different crack propagation problems.

Let us distinguish <u>stable and unstable</u> types of specimen-loading configurations (exemplified in Fig. 2). Namely, we call a configuration stable (unstable), if within the expected range of crack lengths the energy release rate decreases (increases) with the crack growth. Crack arrest is expected for a stable configuration, whereas an avalanche-like crack propagation occurs

in an unstable case when either the crack or the load reaches certain critical value. We turn to separate treatment of these cases.

Stable Case. Let us consider a prenotched specimen (see Fig. 2a) and the probability $P(\vec{X})$ that a crack growing from the notch passes through $\vec{X}$. Apparently, $P(\vec{X})$ is related to the crack propagator (note the position of the coordinate system):

$$P(\vec{X}) = P(\vec{0},\vec{X}) \quad . \tag{9}$$

It is immediate from Eqs. (7a-c), that $P(\vec{X})$ is the solution of

$$\partial_{X_1} P(\vec{X}) = \frac{D}{2} \partial^2_{X_2} P(\vec{X}) - \frac{1}{r} U(\vec{X}) P(\vec{X}) \tag{10a}$$

$$P(\vec{x})\Big|_{X_1 = 0} = \delta(X_2) \tag{10b}$$

$$P(\vec{X}) \to 0 \ , \quad \text{as} \quad X_2 \to \pm \infty \ , \quad X_1 > 0 \quad . \tag{10c}$$

Eq. (10a) was called 'crack diffusion equation' in Ref. 1.

The probability density $p_a(\vec{X})$ for the arrest crack tip location can be expressed in terms of $P(\vec{X})$ and $U(\vec{X})$. Indeed, the probability $p_a(\vec{X})\, dX_1\, dX_2$ of the crack being arrested in a vicinity $dX_1\, dX_2$ of $\vec{X}$ equals the probability $P(\vec{X})\, dX_2$ of reaching the vicinity times the conditional probability $U(\vec{X})\, dX_1/r$ of being arrested upon getting there. Hence

$$p_a(\vec{X}) = P(\vec{X})\, U(\vec{X})/r \tag{11}$$

Unstable case. Let us consider a specimen-loading configuration with a pre-existing crack ω_o (its tip at $\vec{x}$) shown in Fig. 2b. By specimen's failure we mean extension of the crack to the opposite edge. The event of failure is the sum of events consisting of crack extension to an arbitrary point

(B,X_2). For the single path fracture, these events are mutually exclusive. Hence the probability $P_{\omega_0}(\vec{x};\sigma)$ of failure under a given load σ can be expressed through crack propagator $P_{\omega_0}(\vec{x},(B,X_2))$, which represents the probability (density in X_2) of crack extension to (B,X_2):

$$P_{\omega_0}(\vec{x};\sigma) = \int_{\infty}^{\infty} P_{\omega_0}(\vec{x},(B,X_2))\, dX_2 \quad . \tag{12}$$

It is immediate from Eqs. (7a-c) that $P_{\omega_0}(\vec{x};\sigma)$ is the solution of (suppressing σ,ω_0)

$$\partial_{x_1} P(\vec{x}) = \frac{D}{2}\,\partial_{x_2}^2 P(\vec{x}) + \frac{1}{r}\, U(\vec{x})\, P(\vec{x}) \tag{13a}$$

$$P(\vec{x})\Big|_{x_1 = B} \equiv 1 \tag{13b}$$

$$\partial_{x_2} P(\vec{x}) \to 0 \ , \quad \text{as} \quad x_2 \to \pm\infty \ , \quad x_1 < B \ , \tag{13c}$$

We will refer to Eq. (13a) as 'backward crack diffusion equation' (unstable case) and to Eq. (10a) as 'forward crack diffusion equation' (stable case).

Probability of failure $P_{\omega_0}(\vec{x};\sigma)$ can also be interpreted as the distribution of critical loads. Namely, if the precracking is given and the critical load σ_c is the only random variable, then its distribution function is given by

$$F_{\sigma_c}(\sigma) = P_{\omega_0}(\vec{x};\sigma)\Big|_{\vec{x};\omega_0} \tag{14}$$

The probability of failure also yields the conditional probability density $p_c(\vec{x})$ of critical crack tip location. Let us, for example, consider slow crack growth under fatigue or creep. Then the probability $p_c(\vec{x})\, dx_1\, dx_2$ that the crack turns unstable in a vicinity of the point x equals the prob-

ability $h(\vec{x})\ dx_2$ that the slow crack passes through the vicinity times the probability $U(\vec{x})\ dx_1/r$ that it is not critical within the vicinity times the probability $P(\vec{x};\sigma)\big|_\sigma$ that it turns unstable immediately upon leaving the vicinity, i.e.

$$p_c(\vec{x}) = h(\vec{x})\ U(\vec{x})\ P(\vec{x},\sigma)/r\Big|_\sigma \quad . \tag{15}$$

Probability distributions $p_c(\vec{x})$ above and $p_a(\vec{x})$ (Eq. (11)) might be called probability clouds of crack arrest and critical crack tip locations, respectively.

REFERENCES

[1] A. Chudnovsky and B. Kunin, J. Appl. Phys., Vol. 62 (10), 1987.

[α] This assumption is well supported by observations of crack propagation under fatigue and creep conditions. It is often not valid for impact loading.

[β] I. M. Gelfand and A. M. Jaglom, Russ. Math. Surv., Vol. 11, 48 (1956); see also Ref. 1, Section IV, first paragraph.

[γ] M. A. Mull, A. Chudnovsky, and A. Moet, Phil. Mag. A, Vol. 56, 3 (1987), pp. 419-43; A. Chudnovsky and P. C. Perdikaris, in Fourth International Conference on Applications of Statistics and Probability in Soil and Structural Engineering, University of Florence, Italy, 1983 (Pitagora, Bologna, 1983).

[δ] M. R. Leadbetter, G. Lindgren, and H. Rootzen, Extremies and Related Properties of Random Sequences and Processes (Springer, New York, 1983).

[ε] Note that $P\{2\gamma > J_\omega(\xi_1)\} = 1 - F\ (J_\omega(\xi_1)/2)$, where $F(\gamma)$ is given by Eq. (4).

[ζ] It is not an innocent or obvious procedure. The limitations of such an approximation belong to the elasticity theory and will be discussed elsewhere.

[θ] The relation of the dimensionless function U to the function V introduced in Ref. 1, Sec. IV is $U = rV$.

[η] This result can be found in the original papers M. Kac, in Proceedings of the 2nd Berkeley Symposium on Mathematical Statistics and Probability, Berkeley, 1950, edited by J. Newman (Univ. of California Press, Berkeley, 1951) - regarding Eq. (6a), and E. B. Dynkin, Ukranian Math. J., Vol. 6, 21 (1954) (in Russian).

[ι] More precisely, $P(\vec{X})$ is a density with respect to X_2.

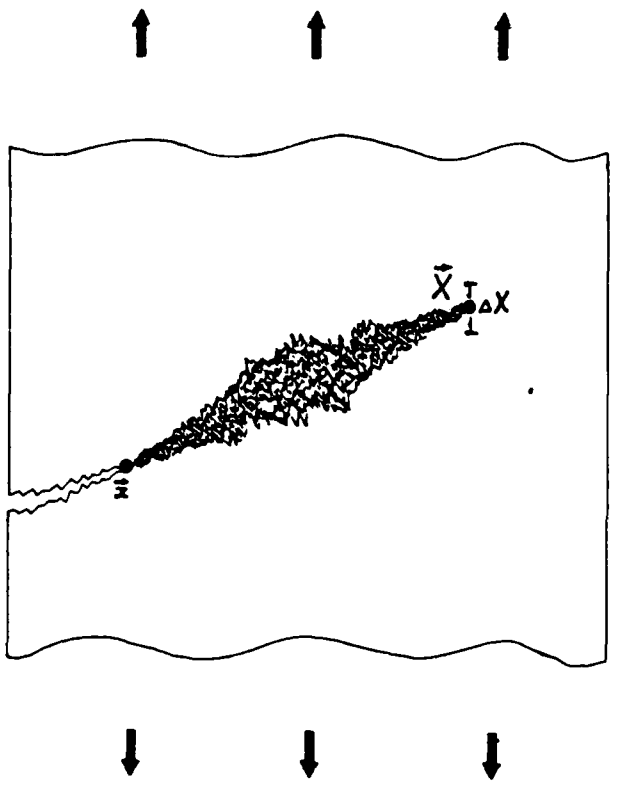

Figure 1.

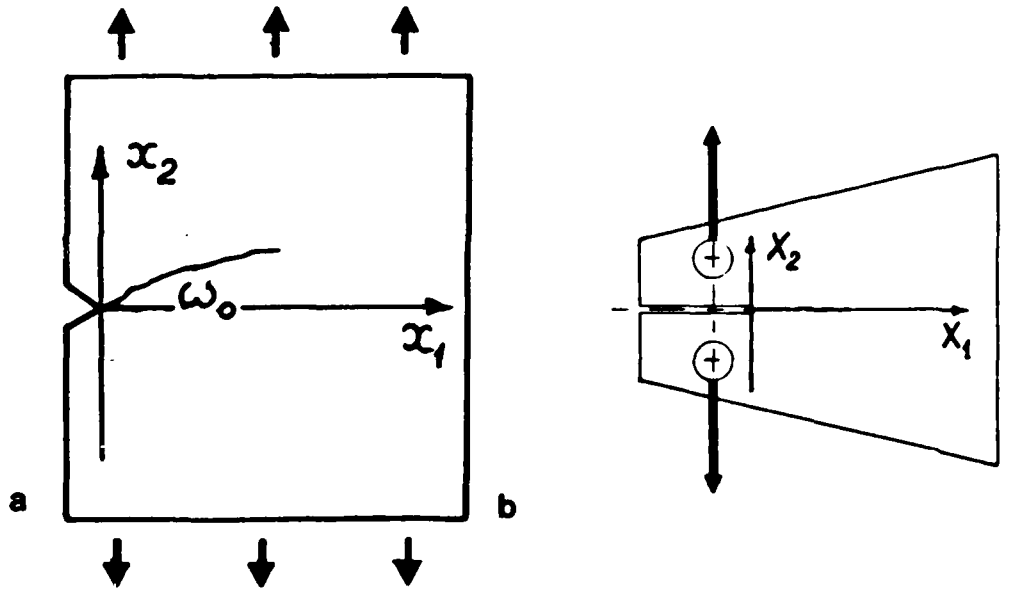

Figure 2.

CHAPTER III

DETERMINATION OF RANDOM STRENGTH FIELD PARAMETERS FROM CRACK ARREST EXPERIMENT

R. Dearth, H. Aglan and A. Moet
Department of Macromolecular Science
Case Western Reserve University
Cleveland, Ohio 44106

and

B. Kunin and A. Chudnovsky
Department of
Civil Engineering, Mechanics, and Metallurgy
University of Illinois at Chicago
Chicago, Illinois 60680

1. Introduction
2. Experimental Procedure
3. Results
4. Theoretical Considerations
5. Data Processing

Introduction

A probabilistic model to extract the strength field parameters, γ^* and α, of a material during brittle crack formation has been developed [1,2]. For a crack arrest experiment the probability of crack penetration depth f(X) at a displacement (δ) is expressed as

$$f(X) = \int_0^{\bar{\delta}} f(\delta)\ f(X|\delta)\, d\delta \tag{1}$$

where $f(\delta)$ is the probability density of the displacement at the grips. Both the f(X) and $f(\delta)$ can be obtained from the results of a crack arrest experiment. The function $f(X|\delta)$ is a conditional probability density of X for a given value of δ. This function is expressed in the form

$$f(X|\delta) = dF(X|\delta)/dX \tag{2}$$

where

$$F(X|\delta) = 1 - \exp\left\{ - \int_{\chi_{notch}}^{\chi} \exp\left[-\left(\Gamma\left(1 + \frac{1}{\alpha}\right) \frac{J_o(\chi;\, \delta)}{2\gamma^*} \right)^{\alpha} \right] \frac{d\chi}{r_o} \right\} \tag{3}$$

where $\Gamma(1 + 1/\alpha)$ is the Gamma function, r_o is the radius of correlation of the material and $J_o(\chi;\delta)$ is the energy release rate for a straight horizontal crack of the same depth χ. γ^* and α are the strength field parameters which characterize the resistance of the material to brittle crack formation.

The utilization of this model involves a minimumization technique to equate or minimize the difference between the experimentally found $f(X)_{ex}$ and the theoretically calculated $f(X)_{th}$. To obtain the theoretical function $f(X)_{th}$, a value of the radius of correlation r_o, for the material, has to be found and incorporated into Eq. 3. Different values of γ^* and α should be tried in the minimumization program until $f(X)_{th} \approx f(X)_{ex}$.

The values of γ^* and α at which the equality condition takes place are the strength field parameters of the material.

In order to demonstrate the utility of this theory an experiment on a model material (PMMA) was conducted. This chapter outlines experimental and analytical techniques to determine the strength field parameters, γ^* and α, of PMMA.

2. Experimental Procedures

The material used in this study is PMMA ("plexiglas M") manufactured by the Rohm and Haas Company(Philadelphia) in the form of 6 mm thick sheets. The reported tensile strength of this grade PMMA is 68.95 x MN/m^2 with a modulus of elasticity of 3.1 GN/m^2.

Twenty-five identical tapered double cantilever beam specimens were machined to the dimensions given in Fig. 1. A saw cut notch of 6 mm was machined into the specimen. The stress intensity factor of this geometry is given by [3]

$$K_I(X;\delta) = \frac{E\delta}{2}\,\frac{k(x)}{S(x)} \tag{4}$$

and

$$R(X) = \begin{cases} \dfrac{2.98}{\left[0.3(\lambda+0.833)\right]^{\frac{1}{2}}}\left(\dfrac{\lambda}{0.3(\lambda+0.833)}+0.7\right) & \text{for } \lambda \le 0.6 \\[2ex] \dfrac{0.537+2.17\left(\left(1+\lambda\right)/\left(1-\lambda\right)\right)}{W^{\frac{1}{2}}(1-\lambda)^{\frac{1}{2}}} & \text{for } \lambda > 0.6 \end{cases}$$

and

$$S(X) = \begin{cases} 328.9\left[\dfrac{3.33Z\lambda + 2.082}{2(\lambda + 0.833)^2} + \dfrac{0.350}{\lambda + 0.833} + 1.464\ln(\lambda + .833) - 1.652\right] & \text{for } \lambda \le 0.6 \\ \dfrac{4.709(4\lambda - 2)}{(1-\lambda)^2} + \dfrac{4.662}{1-\lambda} - 2.666\ln(1-\lambda) + 11.187 & \text{for } \lambda > 0.6 \end{cases}$$

where $\lambda = X/W$ and W is the specimen width measured from the load line.

A razor blade was inserted into the root notch to a depth of 0.5 mm. The total length of the initial notch X_o was 6.5 mm. The experiment was conducted on an Instron 1125 testing machine. The sample was first preloaded to 50 N to properly align the sample and remove any slack in the loading assembly. A monotonically increasing load at a cross-head rate of 0.5 mm/min was applied until the crack jumped from the tip of the razor notch. Immediately after the crack jumped, the cross-head was stopped. At this point, a finite amount of load remained on the specimen due to the remaining ligament. Once this load stabilized, the load was reapplied until failure occurred.

Fractographic analysis was conducted on the fracture surface of the specimen using optical and scanning electron microscopy. From this analysis the crack arrest lengths were measured and elementary fracture events which can be employed as a candidate radius of correlation were identified.

Analysis of the crack diffusion requires the tracing of the twenty-five crack trajectories. One half of each broken specimen was properly aligned and analyzed using a Bendix linear profile system. The crack trajectory along the middle of the fracture surface was traced for each specimen, and magnified 50 times vertically and 5

times horizontally. This is in order to enhance the diffusive features of crack propagation.

3. Results

The results of the present experiment consist of three parts. These are a) Fracture Mechanics of Crack Arrest, b) Fractographic Analysis and c) Crack Diffusion Analysis.

a) Fracture Mechanics of Crack Arrest

A typical load displacement curve is shown in Fig. 2. The grip displacement δ is measured from zero, along the displacement axis, to the point at which the load drops sharply. The values of δ for the twenty-five specimens range from 0.3 mm to 0.6 mm. The histogram representing the probability density of the grip displacement $f(\delta)$ is shown in Fig. 3. The crack arrest length X, also ranges form 10 mm to 40 mm. A histogram representing the probability density of the crack arrest lengths f(X) is shown in Fig. 4.

The energy release rate for a straight horizontal crack of the same depth as that of a corresponding diffusive crack is expressed as

$$J_o = \frac{K_I^2}{E} \tag{5}$$

where K_I is obtained from Eq. 4. The displacement of the grips δ in Eq. 4 has been taken as the average value. The effect of Poisson's ratio due to plane strain contribution (less than 10%) was neglected. The value of J_o for the specimen as a function of the crack depth X is plotted in Fig. 5 for the purpose of illustration. An average value of $J_o = 2\gamma(G) = 363$ J/m^2 was obtained for this grade of PMMA. This value agrees reasonably well with those quoted in the literature; 330 J/m^2 [4] and 400 J/m^2 [5].

b) Fractographic Analysis

A reflected light micrograph of the fracture surface is displayed in Fig. 6. Three distinct regions are evident; "ribs", "mirror" and "river bed" are observed. These fracture surface features have been previously identified [6-8]. SEM examination of the rib region reveals that the distance between the two consecutive ribs is almost constant (0.1 mm) for all specimens as shown in Fig. 7. Hence, this dimension appears as a reasonable candidate for the radius of correlation called upon by Eq. 3.

c) Crack Diffusion Analysis

A trace of the twenty-five crack trajectories superimposed on the specimen geometry is shown in Fig. 8. The trajectories exhibit both a deterministic forward "movement" due to the applied stresses and fluctuations in the y direction due to the varying strength field. This is very similar to Brownian diffusion paths, in which particles make forward movement due to a concentration gradient with random fluctuation along the way. Hence, the variance of the distribution should increase linearly with the crack length X (time in Brownian motion). In Fig. 9 the variance of the Y distance of the trajectories is plotted versus the corresponding crack length X. The plot is a good linear fit. The slope of this line is the diffusion coefficient, D, which reflects the tendency of crack trajectories to deviate from the X axis. This type of analysis has previously been used for a Kevlar polyester composite [9]. Evaluation of D uniquely determines the set of all possible crack trajectories. It is found that the value of the diffusion coefficient for this material, using the present geometry and loading conditions, is 4.22 mm. This difussion coefficient will not be utilized in the present theoretical treatment; being a zeroth approximation, but will be used in further studies.

4. Theoretical Considerations

The outcome of the experiment, described in Section 3, is a pair of random variables: the displacement at the grips, δ, at the instance of crack jump and the crack arrest depth, X, after the jump.

The joint probability density of δ and X is given by:

$$f(X, \delta) = f(\delta) \cdot f(X|\delta) \tag{6}$$

where $f(\delta)$ is the probability density of δ and $f(X|\delta)$ is the conditional probability density of X, for a given value of δ.

The distribution of δ is controlled by the local conditions at the notch tip. This is approximated by a normal distribution, as is suggested by the experimentally observed distribution (Fig. 3).

The theoretical model provides the conditional probability distribution of crack arrest depths, X, for a given displacement δ at the grips. Namely, the corresponding conditional distribution function $f(X|\delta)$ is written as,

$$f(X|\delta) = 1 - \int_{\Omega} \exp\left\{ - \int_{x_o}^{x} U(\chi, \omega(\chi)|\delta) \frac{d\chi}{r_o} \right\} d\mu_X^{(D)}(\omega) \tag{7}$$

Recall that the relationship between $F(X|\delta)$ and the conditional probability density function, $f(X|\delta)$, is

$$f(X|\delta) = dF(X|\delta)/dX \tag{8}$$

Here, in Eq. 7, the functional (outer) integral represents averaging over the space Ω of all possible crack trajectories ω beginning at the notch (X). The exponential term, which is averaged, represents the probability that the crack penetrates to a depth of at least X, if it "chooses" a particular path $y = \omega(\chi)$. The parameter r_o is the correlation distance of the random strength field γ. The function $U(\chi, \omega(\chi)|\delta)\, d\chi/r_o$ represents the probability of crack arrest between depth X and X+dX, provided that the crack "chooses" to propagate along $y = \omega(\chi)$. This function U

is

$$U(\chi, \omega(\chi)\,1\delta) = \exp\left[-\left(\Gamma\left(1+\frac{1}{\alpha}\right) \frac{J(\chi, \omega(\chi); \delta)}{2\gamma^*} \right)^{\alpha} \right] \tag{9}$$

where $\Gamma\,(1+1/\alpha)$ is the gamma function, $J(\chi, \omega(\chi); \delta)$ is the energy release rate for a crack that reaches the depth X along a path ω (for a given displacement δ at the grips), and $\gamma^*>0$, $\alpha>0$ are the strength field parameters to be evaluated. The meaning of γ^* being, the average value of the γ-field, that is assumed statistically homogeneous. The term $d\mu_X^{(D)}(\omega)$ in Eq. 7 is a Wiener Measure [1].

Thus, the joint probability density function for X and δ depends on the parameters γ^* and α, i.e., $f(X,\delta) = f(X,\delta; \gamma^*, \alpha)$.

The probability density function describing the distribution of crack arrest depths, is also needed. This is

$$f(X; \gamma^*, \alpha) = \int_0^{\infty} f(X,\delta; \gamma^*,\alpha)\, d\delta$$

$$= \int_0^{\infty} f(\delta)\, f(X \mid \delta; \gamma^*, \alpha)\, d\delta \tag{10}$$

The parameters γ^* and α, can now be found by "comparing" the theoretical distribution of crack arrest depths given by Eq. 10, to the experimental distribution, using the least square fit method (a version of the maximum likelihood principle).

The functional integral in Eq. 7, through which $f(X; \gamma^*, \alpha)$ is ultimately expressed, can be evaluated by different approximations.

The zeroth approximation is the one which approximates the energy release rate $J(\chi, \omega(\chi); \delta)$ in Eq. 9, for a crack that follows a path ω to a depth χ by the energy release rate $J_o(\chi; \delta)$ for a straight horizontal crack of the same depth χ. The resulting expression for the conditional distribution function of the crack arrest depths $F(X|\delta)$ is

now,

$$F(X|\delta) = 1 - \exp\left\{ - \int_{x_o}^{x} \exp\left[- \left(\Gamma\left(1 + \frac{1}{\alpha}\right) \frac{J_o(\chi;\delta)}{2\gamma^*} \right)^{\alpha} \right] \frac{d\chi}{r_o} \right\} \tag{11}$$

5. Data Analysis

The experiment yielded twenty-five pairs of values; X_i, δ_i, $i = 1,\ldots,25$ (X_i is the crack arrest depth in the i-th specimen and δ_i is the displacement of the grips at the instance of the crack jump in the i-th specimen).

First, the points (χ_i, δ_i) were placed in the X, δ-plane, Fig. 10. Two points were excluded from the set of twenty-five due to their general non-conformity with the remaining points, resulting in a total number of twenty-three experimental points.

The histogram of the probability density of δ was approximated by a normal distribution using the least square fit.

$$f(\delta) = \frac{1}{\sigma\sqrt{2\pi}} \exp\left[- \frac{(\delta - \langle\delta\rangle)^2}{2\sigma^2} \right] \tag{12}$$

where $\langle\delta\rangle = \frac{1}{23} \sum_{i=1}^{23} \delta_i$

Both the histogram and the normal distribution fit are shown in Fig. 11. The normal distribution is used as a matter of convenience. In what follows, the histogram could have been used directly; a step-function form of the probability density function for δ.

The "Griffith" $\gamma^{(G)}$ was determined from the equation

$$2\gamma^{(G)} = \frac{1}{23}\sum_{i=1}^{23} J_o(X_i;\delta_i) \tag{13}$$

This is a natural choice for the initial value of $2\gamma^*$ in an interative algorithm of finding the least square fit values γ^*_{fit}, α_{fit}. A value of $2\gamma^{(G)}$ was found to be 363 J/m^2 and used as an initial value for $2\gamma^*$.

The experiment comprises 23 specimens. This is a relatively small sample to construct a detailed histogram of the crack arrest depth. Obviously, the histogram in Fig. 4 is not sufficiently adequate. Hence, a more tedious procedure was used. The range of crack arrest depth (11-39 mm) was subdivided into seven intervals, 4 mm each. Every data point was assigned a weight 1/23. This weight was distributed homogeneously over an auxiliary 4 mm interval centered at the data point, i.e., the density of an individual point is

$$\frac{1}{23x4}\left(m^{-1}\right)$$

Therefore, the weight of each point is subdivided between two adjacent intervals. The total weight accumulated in every one of the seven intervals yields the histogram value.

Differentiating the function F(X|δ) in Eq. 11 with respect to X given rise to the conditional probability function f(x|δ). For different initially assumed values of γ^* and α (r_o is constant = 0.1 mm), the theoretical values of f(X|δ) were obtained. The probability density function of crack arrest depth f(X) was then obtained from Eq. 10.

Finally the Levenberg-Marquardt alogirthm of non-linear least squares fit was applied to match theoretical f(X) to its experimental counterpart (histogram of Fig. 12). Only one solution was found, names $2\gamma^*$ = 47.6 J/m^2 and α = 0.64. The theoretical probability distribution f(X) together with the experimental histogram (Fig. 12) are shown in Fig. 13.

It is noteworthy that the average value of J_o at the crack arrest point (360 J/m^2) falls within the range of values reported in the literature for PMMA [4,5].

In the present model in order for the crack to be arrested at the point X, but not before, means that J_1 should exceed 2γ at all points prior to X. It follows that all peaks of the γ-field ought to be lower than J prior to X. This implies that the average value of γ^* of the field should be lower than the value of J at X. This is schematically illustrated in Fig. 14. The strength field-γ is random as illustrated schematically by the vertical lines. The average strength field is $2\gamma^*$ which is obtained from the probabilistic model. The solid circles in Fig. 14 are points of crack arrest. It is noticed that these conditions occur at higher values of strength field than the average $2\gamma^*$.

Refererences

1. A. Chudnovsky and B. Kunin, J. Appl. Phys., 62, 10, 1987.
2. A. Chudnovsky and B. Kunin, to be published.
3. Y. Murakami, (Ed.), "Stress Intensity Factors Handbook," Pergamon Press, 1987.
4. A. Vandenboogaart: Proceedings of the Physical Basis of Yield and Fracture Conference, Oxford, 167, 1966.
5. L. Broutman and T. Kobayashi, U.S. Army Materials and Mechanics Research Center Report, AMMRC CR 71-14.
6. S. Newman and I. Wolock, J. Appl. Phys., 29, 49, 1958.
7. R. Kusy, H. Lee and D. Turner, J. Mater. Sci., 11, 118, 1976.
8. W. Doll, J. Mater. Sci., 10, 935, 1975.
9. M. Mull, A. Chudnovsky and A. Moet, Philos. Mag. A 56, 3, 414, 1987.

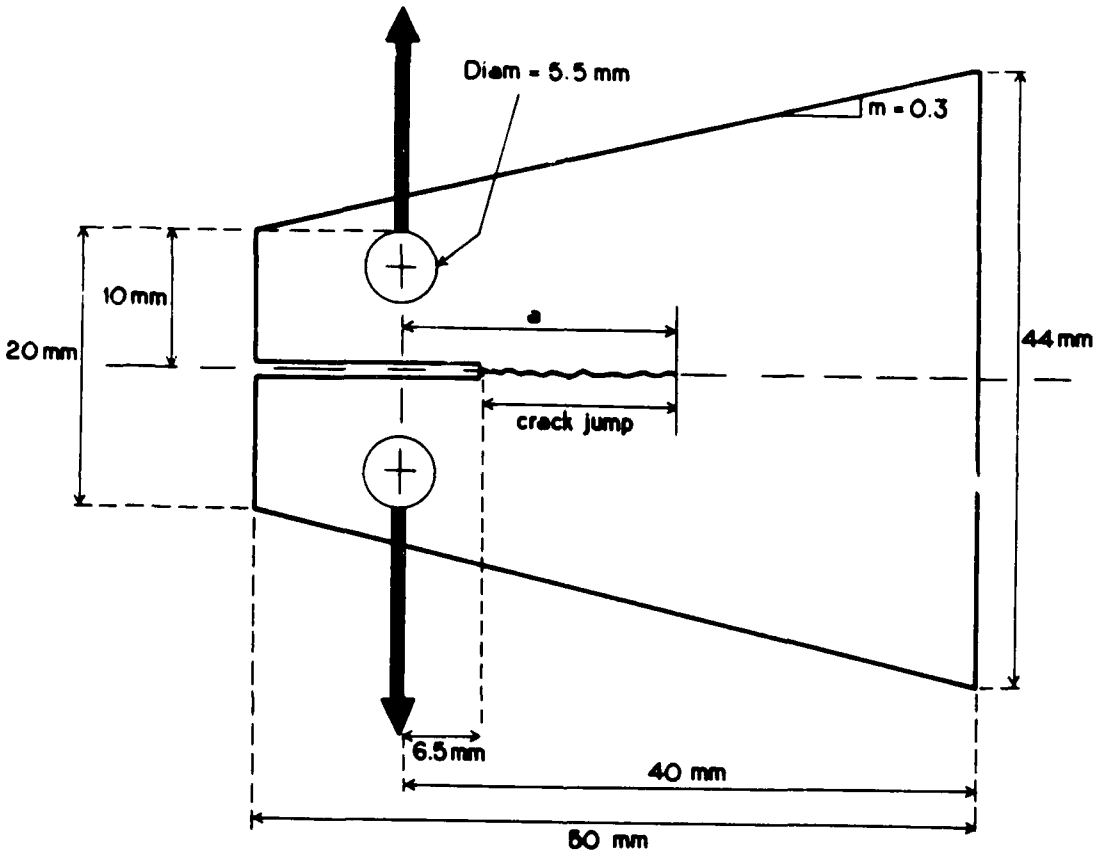

Fig. 1 Sample geometry

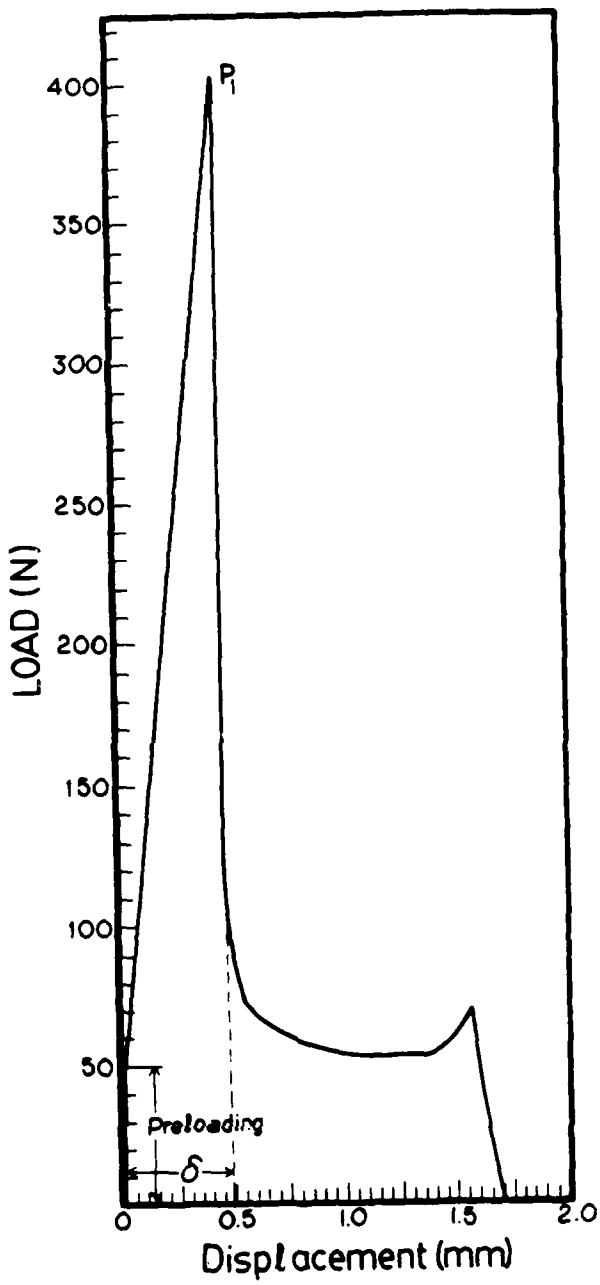

Fig. 2 Typical load-displacement curve

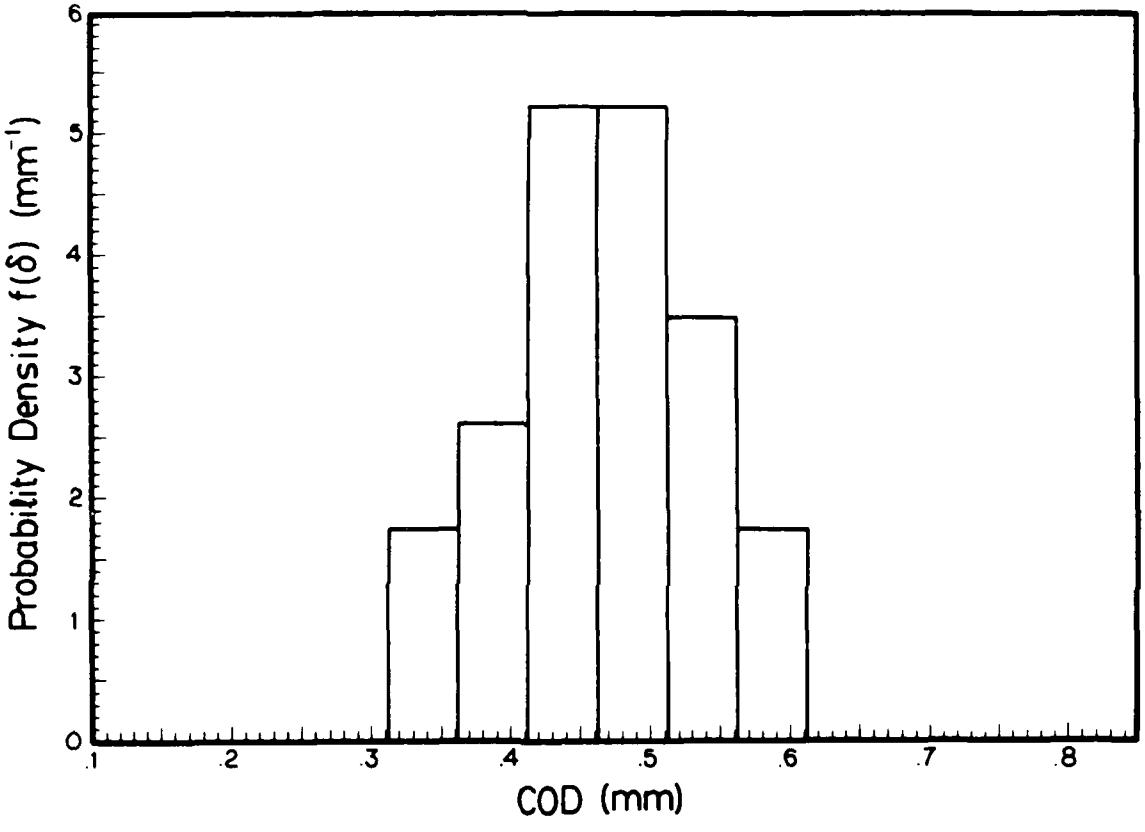

Fig. 3 Histogram of the displacement at the grip δ

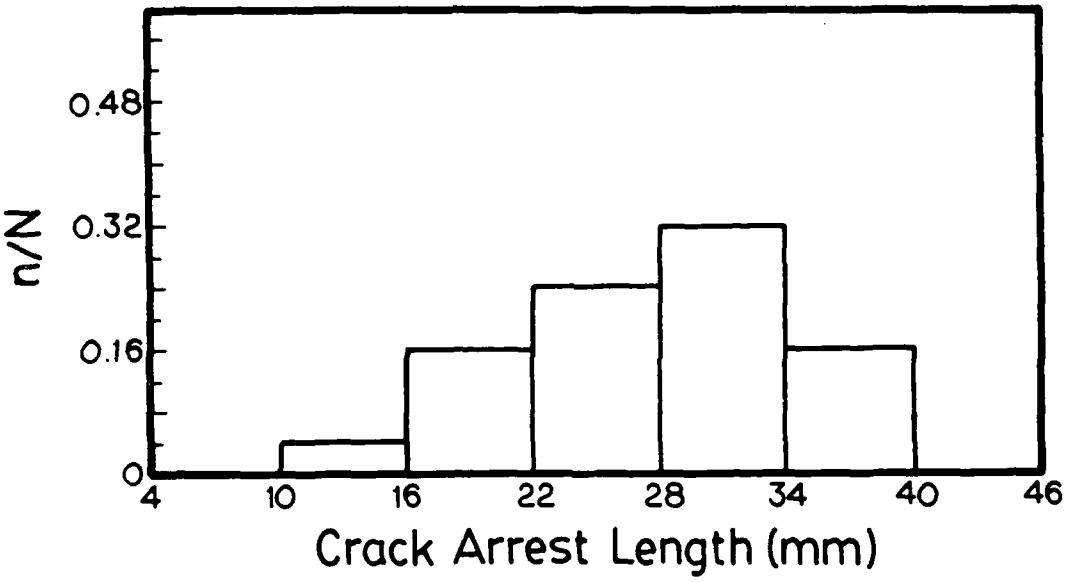

Fig. 4 Histogram of the crack arrest depth X

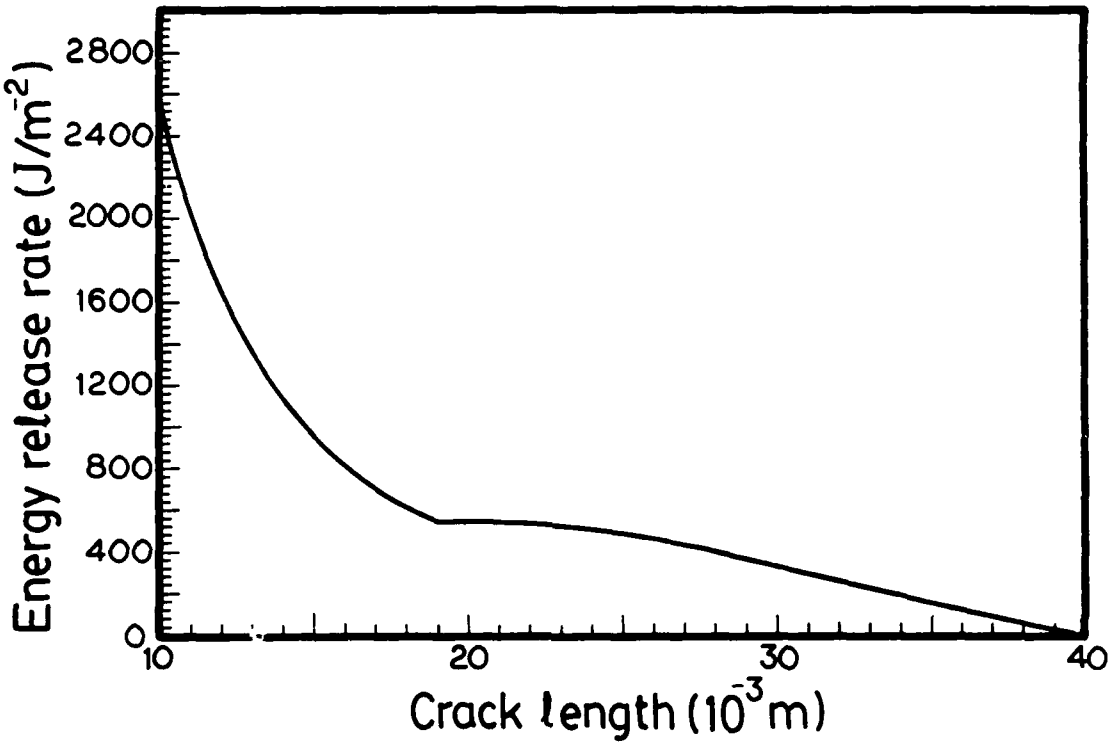

Fig. 5 Energy release rate versus crack length for the tapered specimen

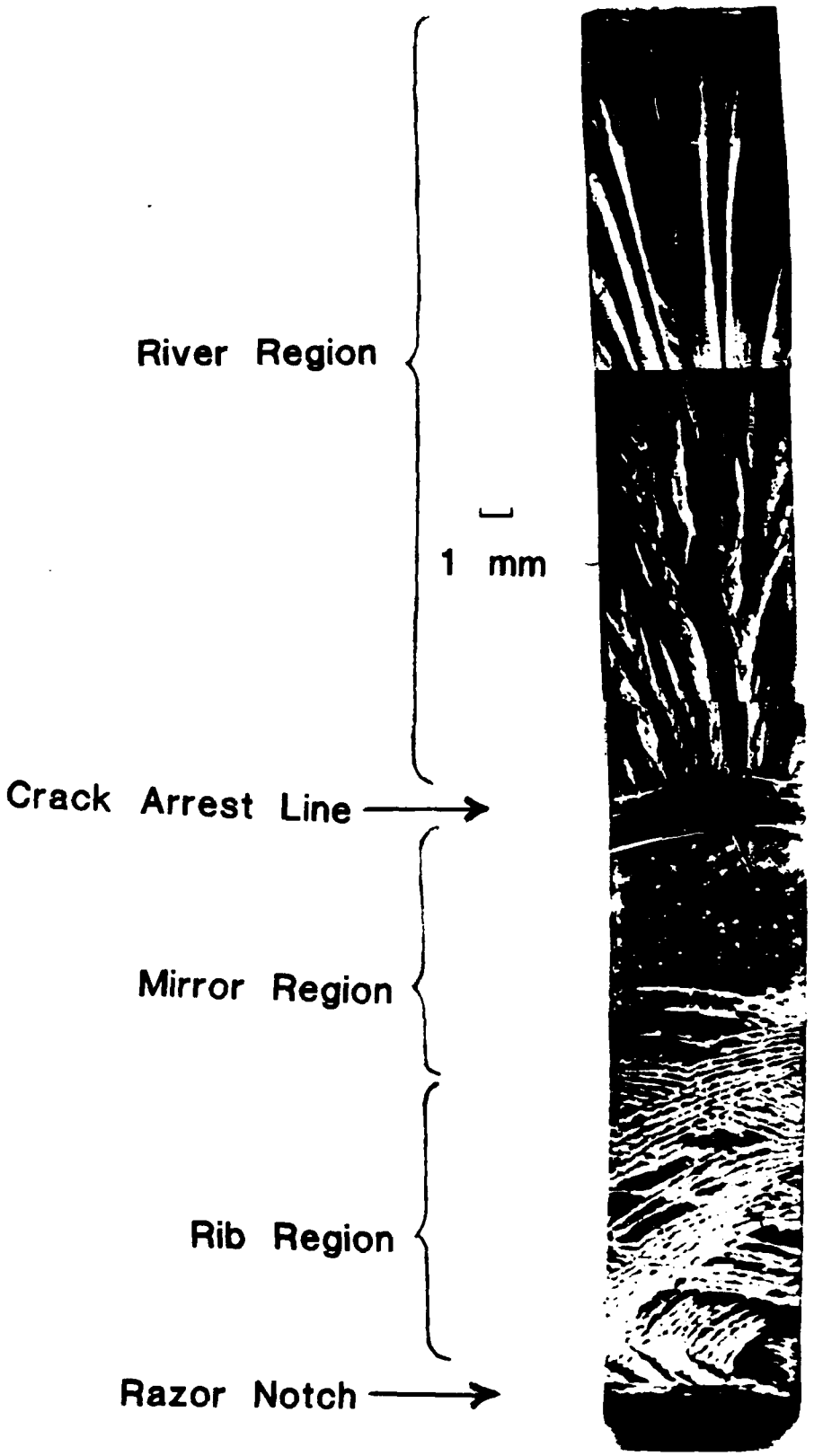

Fig. 6 Fracture surface after tensile failure of a tapered double cantilever specimen

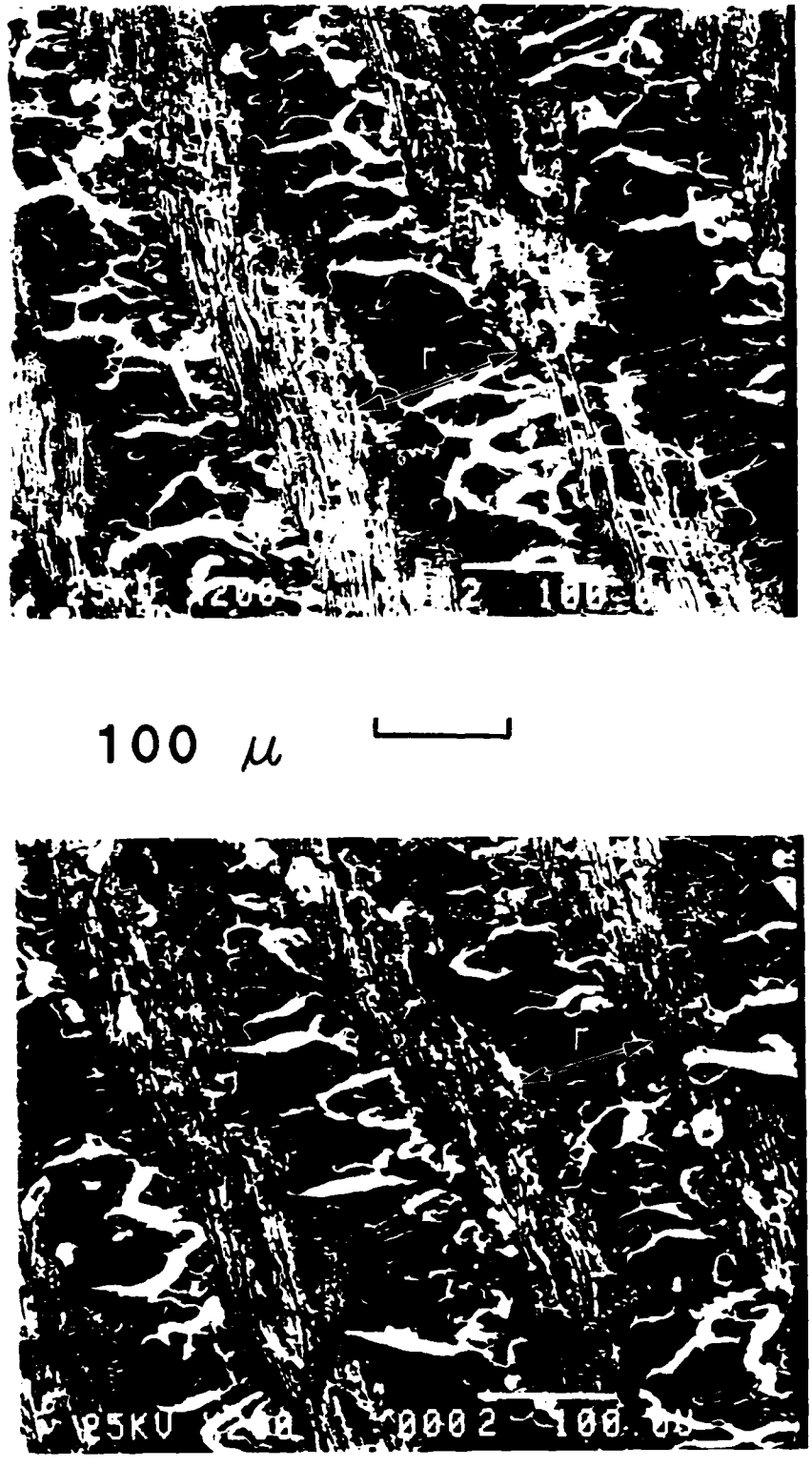

Fig. 7 SEM micrograph of the rib region at different crack lengths

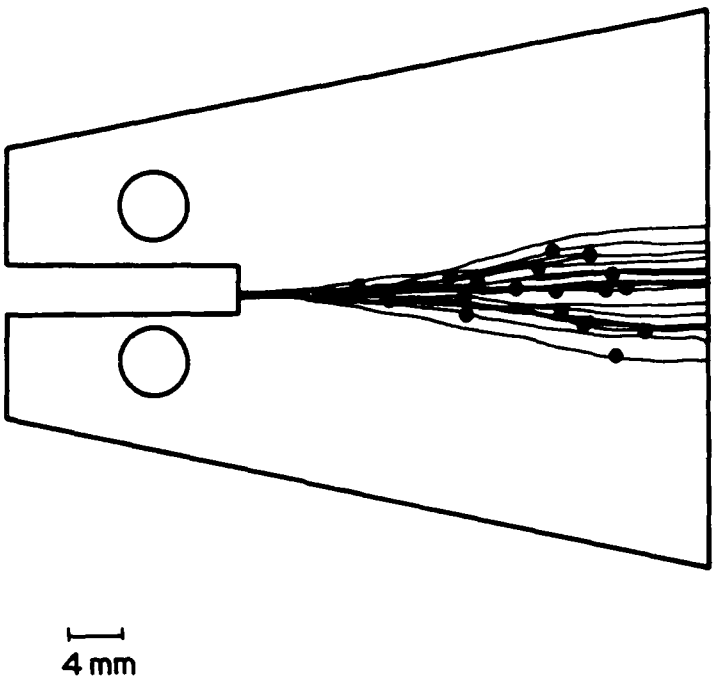

Fig. 8 A set of 25 crack trajectories superimposed on the specimen geometry

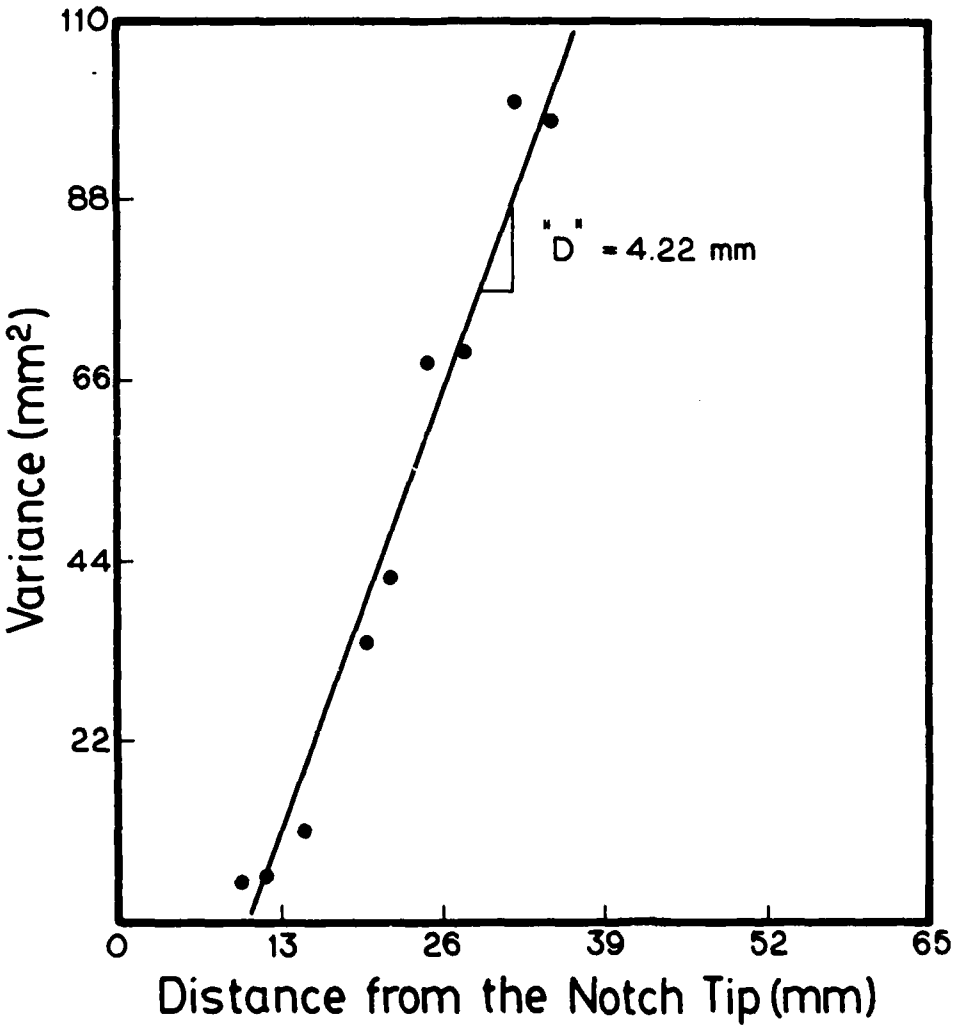

Fig. 9 Variance of crack trajectory as a function of crack length

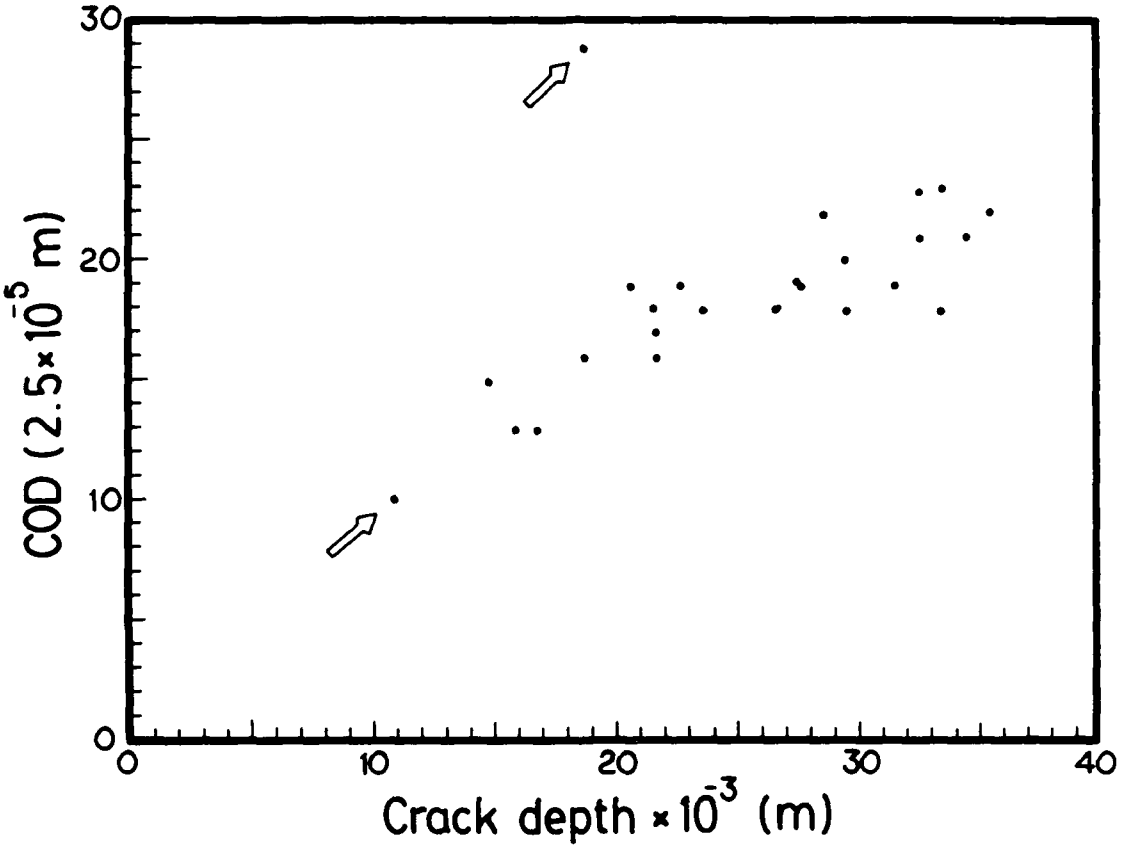

Fig. 10 The crack arrest depth, X, and the displacement at grip for 25 specimens in the X-δ plane

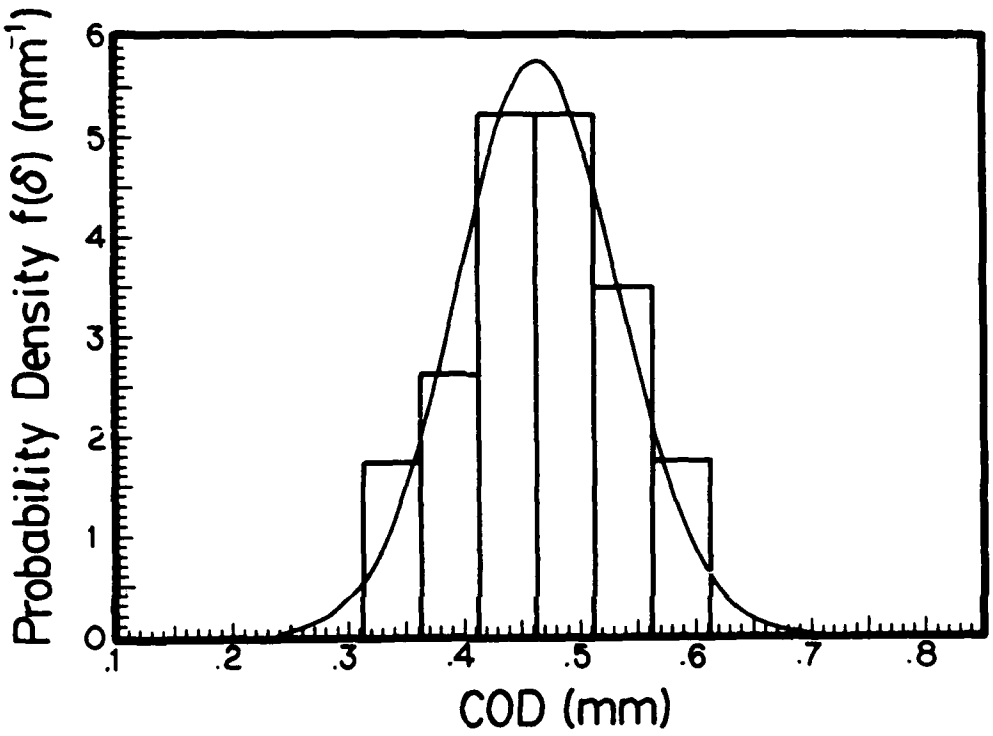

Fig. 11 Histogram of δ and its approximation by a normal distribution

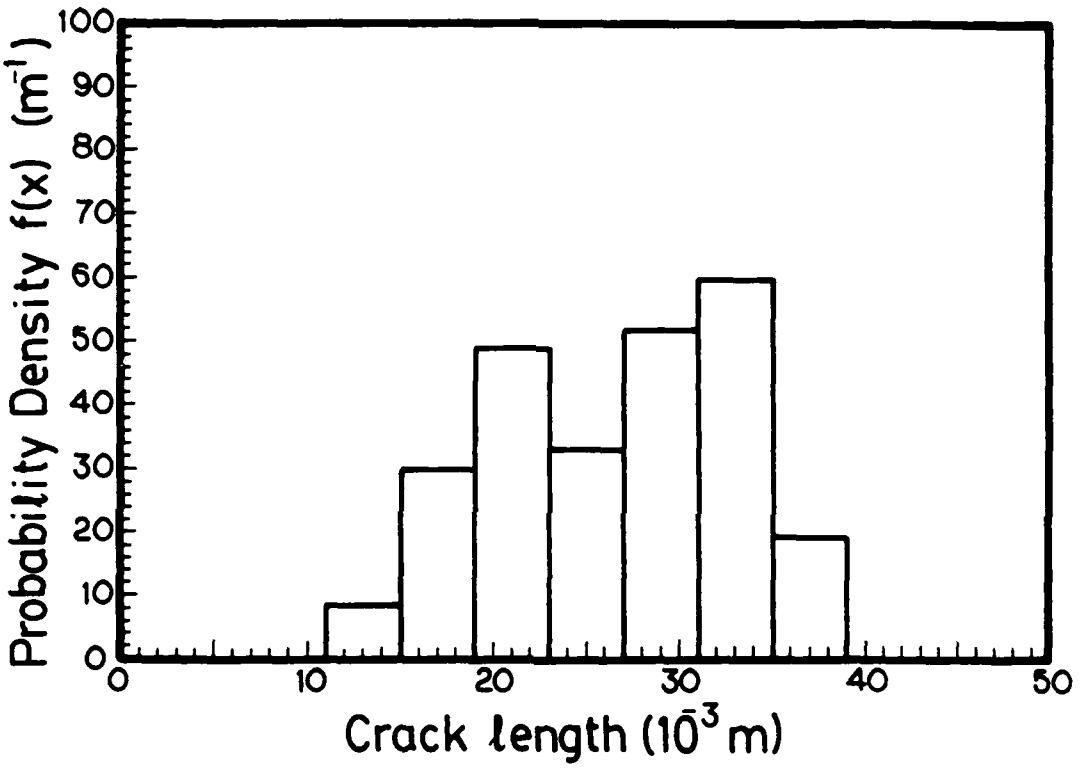

Fig. 12 Histogram of X after points spread treatment

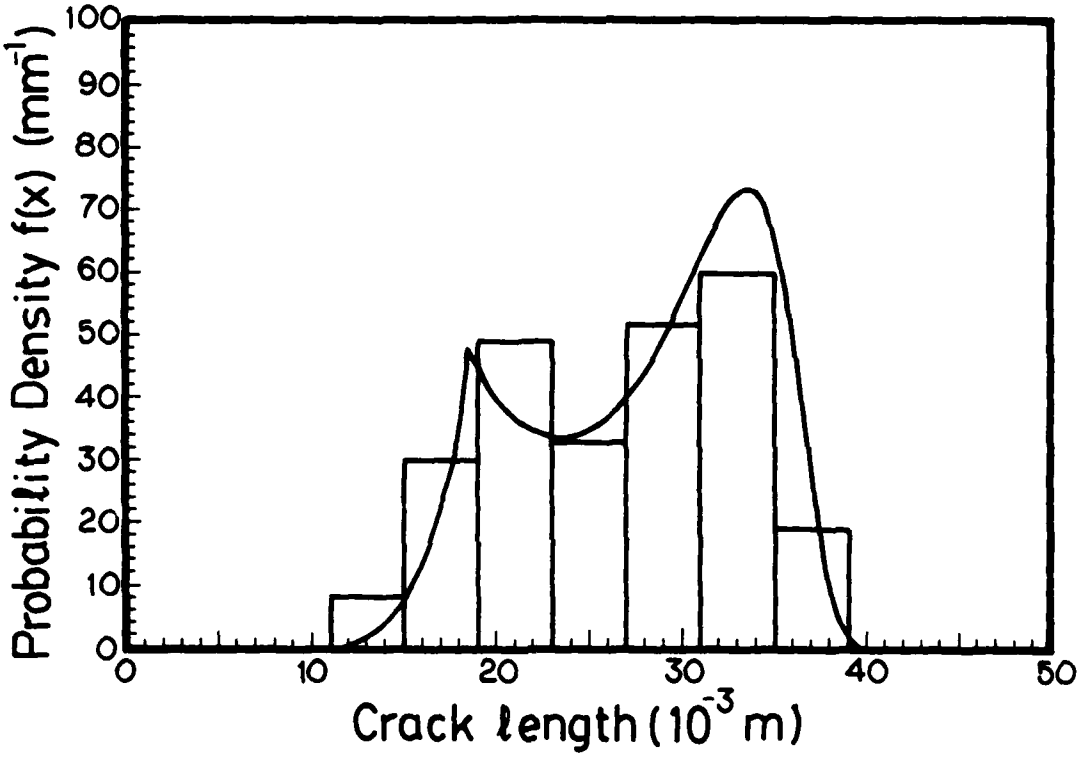

Fig. 13 The theoretically evaluated f(X) superimposed on the histogram in Fig. 12

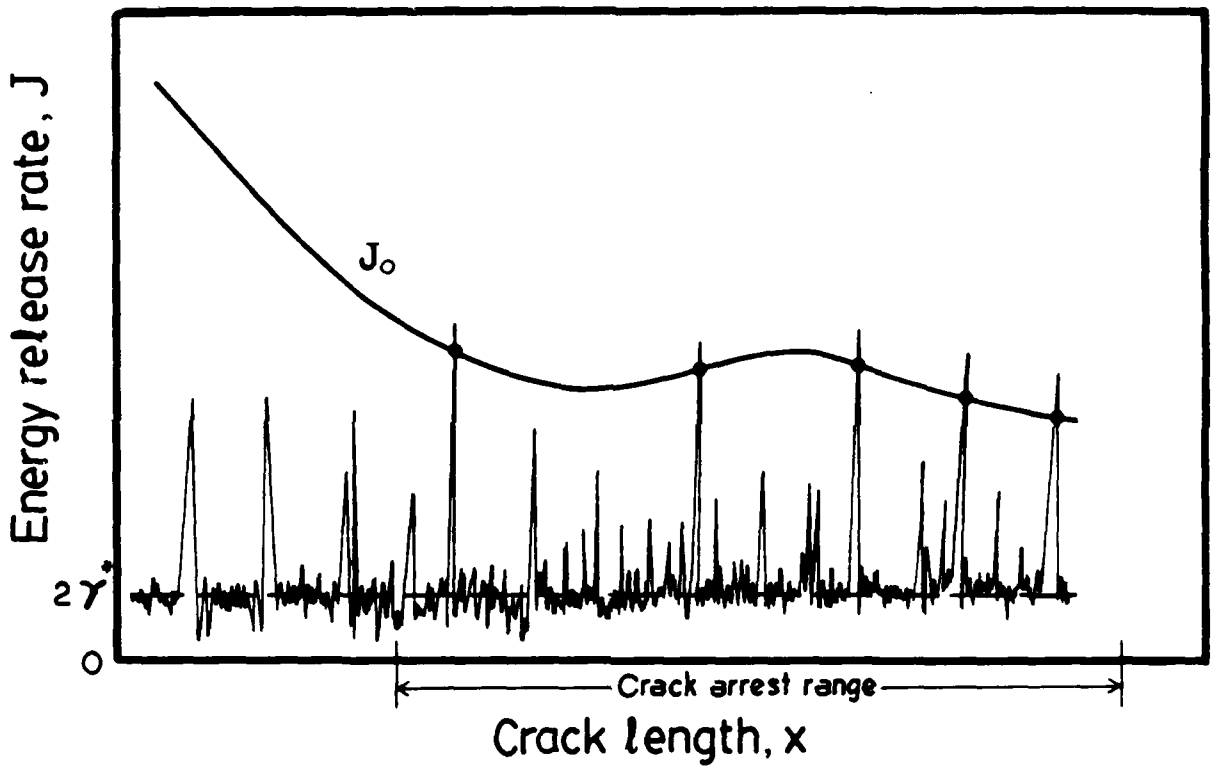

Fig. 14 Schematic illustration of the Υ-field for brittle crack formation based on a crack arrest experiment